Dynamic spatiotemporal variability of alpha-BOLD relationships during the resting-state and task evoked responses

Mayhew, Stephen; Bagshaw, Andrew

DOI:
10.1016/j.neuroimage.2017.04.051

Document Version
Peer reviewed version

Citation for published version (Harvard):
Mayhew, S & Bagshaw, A 2017, 'Dynamic spatiotemporal variability of alpha-BOLD relationships during the resting-state and task evoked responses', *NeuroImage*. https://doi.org/10.1016/j.neuroimage.2017.04.051

Dynamic spatiotemporal variability of alpha-BOLD relationships during the resting-state and task-evoked responses

S.D. Mayhew, A.P. Bagshaw

www.elsevier.com

PII: S1053-8119(17)30369-5
DOI: http://dx.doi.org/10.1016/j.neuroimage.2017.04.051
Reference: YNIMG13992

To appear in: *NeuroImage*

Received date: 23 September 2016
Revised date: 27 March 2017
Accepted date: 21 April 2017

Cite this article as: S.D. Mayhew and A.P. Bagshaw, Dynamic spatiotemporal variability of alpha-BOLD relationships during the resting-state and task-evoked responses, *NeuroImage,* http://dx.doi.org/10.1016/j.neuroimage.2017.04.051

Dynamic spatiotemporal variability of alpha-BOLD relationships during the resting-state and task-evoked responses

Short title: spatiotemporal dynamics of alpha-BOLD relationship

S. D. Mayhew and A.P. Bagshaw

Birmingham University Imaging Centre (BUIC), School of Psychology, University of Birmingham, Birmingham, UK

Corresponding author: Dr Stephen D. Mayhew, Birmingham University Imaging Centre (BUIC), School of Psychology, University of Birmingham, Edgbaston, Birmingham, B15 2TT, UK. Email: s.d.mayhew@bham.ac.uk. Telephone: +441214147191

Key Words: alpha oscillation, BOLD response, dynamic connectivity, spontaneous, prestimulus

Abstract

Accurate characterization of the spatiotemporal relationship between two of the most prominent neuroimaging measures of neuronal activity, the 8-13Hz, occipito-parietal EEG alpha oscillation and the BOLD fMRI signal, must encompass the intrinsically dynamic nature of both alpha power and brain function. Here, during the eyes-open resting state, we use a 16s sliding-window analysis and demonstrate that the mean spatial network of dynamic alpha-BOLD correlations is highly comparable to the static network calculated over six minutes. However, alpha-BOLD correlations showed substantial spatiotemporal variability within-subjects and passed through many different configurations such that the static network was fully represented in only ~10% of 16s epochs, with visual and parietal regions (coherent on average) often opposingly correlated with each other or with alpha. We find that the common assumption of static-alpha BOLD correlations greatly oversimplifies temporal variation in brain network dynamics. Fluctuations in alpha-BOLD coupling significantly depended upon the instantaneous amplitude of alpha power, and primary and lateral visual areas were most strongly negatively correlated with alpha during different alpha power states, possibly suggesting the action of multiple alpha mechanisms. Dynamic alpha-BOLD correlations could not be explained by eye-blinks/movements, head motion or non-neuronal physiological variability. Individual's mean alpha power and frequency were found to contribute to between-subject variability in alpha-BOLD correlations. Additionally, application to a visual stimulation dataset showed that dynamic alpha-BOLD correlations provided functional information pertaining to the brain's response to stimulation by exhibiting spatiotemporal fluctuations related to variability in the trial-by-trial BOLD

response magnitude. Significantly weaker visual alpha-BOLD correlations were found both preceding and following small amplitude BOLD response trials compared to large response trials.

Introduction

The intrinsic electromagnetic oscillations of the brain's neuronal populations are widely studied as functional correlates of cognitive systems. The 8-13Hz alpha oscillation is the dominant characteristic of scalp EEG and the most readily measured electrophysiological signal of human brain activity. The alpha oscillation is a fundamental feature of both spontaneous and task-evoked brain activity and has been shown to play an important role in the perception of external stimuli (Babiloni et al., 2006; Haegens et al., 2011; Handel et al., 2011; Hanslmayr et al., 2007; Hanslmayr et al., 2013; Linkenkaer-Hansen et al., 2004) and many cognitive abilities (Basar et al., 2001; Basar et al., 1997; Jensen et al., 2002; Klimesch, 1999; Mazaheri and Jensen, 2010; Palva and Palva, 2011; Pfurtscheller and Lopes da Silva, 1999; Sauseng et al., 2005; Zumer et al., 2014). It is hypothesised that it provides a mechanism for gating and regulating the flow of information both within and between brain networks by selectively inhibiting task-irrelevant pathways (Jensen and Mazaheri, 2010; Klimesch et al., 2007; Zumer et al., 2014). Alpha is also a commonly used measure of a subject's level of arousal, attention and cortical excitability (Olbrich et al., 2009; Rihs et al., 2007; Rihs et al., 2009; Romei et al., 2008; Roth, 1961; Strijkstra et al., 2003; Thut et al., 2006).

While alpha is therefore clearly an important neural oscillation with considerable behavioural and physiological implications, uncertainty still exists about how it is generated. Partly, this is a result of the difficulty in accurately localising the generators of scalp electromagnetic activity, and also a lack of sensitivity to crucial deep brain structures such as the thalamus. Consequently the relationship between the power of the occipito-parietal alpha oscillation and the amplitude of the blood oxygenation level

dependent (BOLD) fMRI signal has long been of interest for localising the spatial origins of this neuronal activity and the cortical and subcortical regions whose activity is influenced by it. Commonly, this relationship has been assessed by computing the linear correlation between the two signal timeseries. However, the majority of previous studies only assess "static" alpha-BOLD correlations over at least several minutes, often as long as ten minutes (de Munck et al., 2008; de Munck et al., 2009; Goldman et al., 2002; Laufs et al., 2006; Laufs et al., 2003). This neglects both the intrinsic, spontaneous nature of alpha oscillations as well as the dynamic information about temporal fluctuations in brain activity that they contain.

Static negative correlations between spontaneous fluctuations in resting-state alpha power and the BOLD signal have been observed in primary and lateral visual cortex (Ben-Simon et al., 2008; de Munck et al., 2008; de Munck et al., 2007; de Munck et al., 2009; Feige et al., 2005; Goldman et al., 2002; Laufs et al., 2006; Laufs et al., 2003; Liu et al., 2012; Mo et al., 2012; Moosmann et al., 2003; Wu et al., 2010; Zhan et al., 2014) as well as bilateral frontal and parietal regions resembling the dorsal attention network (DAN) (de Munck et al., 2007; Laufs et al., 2006; Mo et al., 2012; Zhan et al., 2014). In addition, positive correlations have been less frequently observed in the bilateral insula (Goldman et al., 2002), the thalamus (de Munck et al., 2007; Feige et al., 2005; Goldman et al., 2002; Liu et al., 2012; Wu et al., 2010) and the default mode network (DMN) (Mo et al., 2012; Wu et al., 2010).

Static alpha-BOLD correlations therefore encompass brain regions from multiple different intrinsic connectivity networks (ICNs) (de Munck et al., 2009; Feige et al., 2005; Goldman et al., 2002; Laufs et al., 2006; Mo et al., 2012). These ICNs are defined

by strong static correlations in fMRI signal between their individual nodes, exhibiting high levels of within-network functional connectivity (Cole, 2010; Van Dijk et al., 2009), with distinct temporal patterns of activity compared to other ICNs, and hence low levels of between-network functional connectivity. By definition therefore different ICNs do not remain continually, coherently active with each other for periods of several minutes and beyond, otherwise they would be classed as the same ICN. Instead, the static alpha-BOLD network, which encompasses multiple ICNs (visual, saliency, DAN, DMN), is composed of dynamic networks that regularly come in and out of coherence with each other over long periods of time (Smith et al., 2012; Zalesky et al., 2014). On average this variable relationship with alpha approximates a common pattern of coupling, but to what extent this common pattern represents the actual regions involved in alpha fluctuations remains to be clarified.

Functional measures of dynamic neuronal interactions can be extracted by studying how the coherence in the activity of different brain regions fluctuates over time. In recent years, there has been an increase in studies implementing short time-windows to assess such temporally fluctuating, functional relationships both within- and between-ICNs (Allen et al., 2014; Chang and Glover, 2010; Gonzalez-Castillo et al., 2014; Handwerker et al., 2012; Hutchison et al., 2013b; Schaefer et al., 2014; Tagliazucchi et al., 2012; Wilson et al., 2015; Zalesky et al., 2014). These dynamic fMRI functional connectivity analyses have revealed that short-term correlations, on the order of tens of seconds, are closer to the dynamic temporal organization of brain activity and therefore more functionally informative, findings supported by recent MEG studies (Betti et al., 2013; de Pasquale et al., 2010).

An analogous dynamic analysis is well suited to studying resting-state alpha-BOLD coupling, due to the transient nature of alpha power fluctuations. A single, static measure of alpha-BOLD correlation can be considered an approximation of the average relationship over a period of ten minutes, but provides little useful functional information about brain dynamics. A dynamic approach would provide an informative tool to investigate the effect of transient alpha-BOLD correlations upon a subsequent task response or a transition between behavioural states. The central hypothesis of the current study is that the commonly reported static relationship between alpha power and visual/DAN/DMN/thalamic BOLD signal is an oversimplification and that these regions show temporal fluctuations in the strength of the alpha-BOLD correlation. It is acknowledged that the spatial location of alpha-BOLD correlation displays a large degree of between-subject variability (Goncalves et al., 2006; Laufs et al., 2006). More recent work has begun to show the potential of dynamic EEG-BOLD correlations to elucidate temporal patterns of resting-state brain connectivity (Chang et al., 2013; Tagliazucchi et al., 2012; Yu et al., 2016), but a basic understanding of the extent and functional significance of within-subject variability in alpha-BOLD coupling remains lacking.

In this study, we conduct a thorough investigation of the spatiotemporal dynamics of correlations between occipito-parietal alpha power and the BOLD signal during the eyes-open resting-state, before applying the method to study how the temporal profile of alpha-BOLD correlations fluctuates with variations in the trial-by-trial amplitude of the BOLD response to visual stimulation. We initially investigate how an individual's alpha power and alpha frequency contribute to the between-subject variability in the strength and spatial pattern of static resting-state alpha-BOLD correlations. We then employ a

sliding window analysis to study the temporal dynamics of the resting-state alpha-BOLD relationship. Firstly, we compare dynamic to static correlations to investigate whether alpha-BOLD correlations can be accurately and meaningfully assessed at short timescales of 60, 32, 16s or 8s (30, 16, 8 or 4 MR samples).

We then investigate if alpha power is consistently correlated with the BOLD signal in the brains major ICNs. We assess how often brain regions that are correlated with alpha on average are actually uncoupled from alpha and from each other, addressing questions such as: whether the spatial pattern of alpha-BOLD coupling passes through different configurations, whether an alpha-BOLD network exists that temporally varies in strength, sometimes showing periods of no correlation at all, or whether it fractures into different components that show structured variations in regional correlations over time.

We use the extra information provided by this dynamic analysis to investigate differences in the spatial pattern and extent of alpha-BOLD correlations between periods of high and low alpha power. Finally, using an additional recording of EEG-fMRI responses to visual stimulation we investigate how the spatiotemporal pattern of dynamic alpha-BOLD correlations relates to the magnitude of the brain's response to stimulation and whether temporal differences in alpha-BOLD coupling are associated with differences in BOLD response amplitude.

Methods

Written informed consent was obtained from all participants and the protocol was approved by the Research Ethics Board of the University of Birmingham. Thirty-two

right-handed subjects (age = 26 ± 4 years, 16 females) took part in a resting-state EEG-fMRI study whereby they were instructed to lie-still and keep their eyes open for 6 minutes.

EEG-fMRI data acquisition

All experiments were conducted at the Birmingham University Imaging Centre (BUIC) using a 3T Philips Achieva MRI scanner. An eight-channel phased-array head coil was used to acquire a T1-weighted anatomical image (1 mm isotropic voxels) and whole-brain T2*-weighted, functional EPI data (180 volumes, 32 slices, 3x3x4 mm voxels, TR=2000 ms, TE=35 ms, SENSE factor=2, flip angle=80°). Subject's cardiac and respiratory cycles were continuously recorded throughout using the scanner's inbuilt pulse oximeter and respiratory belt. EEG data were simultaneously recorded from 62 scalp Ag/AgCl ring-type electrodes distributed according to the 10–20 system (EasyCap, Germany) with two additional channels used for recording the electrocardiogram and electrooculogram. The impedance at all recording electrodes was maintained below 20 kΩ. BrainAmp MR-plus EEG amplifiers (Brain Products, Munich) were used for recording data at 5 kHz with 0.016-250 Hz hardware filters. Subjects were positioned such that electrodes Fp1 and Fp2 were at the magnet isocentre in the foot/head direction so as to minimise the gradient artefact (Mullinger et al., 2011). The EEG acquisition clock was synchronised with the MR scanner clock, with the TR equal to a multiple of the EEG sampling period, to ensure consistent sampling of the artefact waveforms (Mullinger et al., 2008).

Alpha oscillation measurement

EEG data were corrected for MRI gradient and pulse (ballistocardiogram, BCG) artefacts using average-artefact subtraction in Brain Vision Analyser 2 (BrainProducts, Munich). Data were subsequently down-sampled (500Hz), band-pass filtered (1-30Hz) and re-referenced to an average of all non-noisy channels. Separately for each subject, data were then further processed with independent component analysis (fastICA (Hyvarinen, 1999)) to extract the alpha oscillation from other brain processes and background noise (Becker et al., 2011; Mayhew et al., 2013b; Scheeringa et al., 2011b). Lateralised alpha components were not consistently present in all subject's decompositions so we could not separately study the activity of these sources, i.e. compared to central components. Alpha ICs exhibit a small degree of variability between subjects in their spatial topographies, however overall we observed a high degree of consistency, including central posterior topographies along with more lateral regions, which together encompass bilateral occipito-parietal cortex in all cases. The group median average number of alpha components was 4, range 2-6. Scalp topographies of the static alpha power components of 12 representative subjects are shown in Figure S1. Therefore to ensure accurate measurement of the alpha oscillation only ICs with bilateral or lateralized parietal/occipital scalp topography and a clear spectral peak between 8-13Hz were selected and retro-projected into channel space. Data from parietal/occipital channels PO3/4, POz, O1/2 and Oz were then epoched based on the timing of each MRI volume trigger (0-2000ms). For each subject, we then calculated the alpha power topography of every 2s (TR) interval to assess temporal variability in the spatial pattern of alpha power.

To investigate how similar each TR's alpha distribution was to the static distribution, for each subject we then calculated the spatial correlation between their static alpha topography and the alpha topography of each TR period. Time-frequency spectrograms of oscillatory power were calculated for all TR epochs using the continuous Morlet wavelet transform in the Fieldtrip toolbox (http://fieldtrip.fcdonders.nl/) (Oostenveld et al., 2011). The mean alpha power of each TR epoch was calculated between ±1Hz of each individuals' alpha frequency (IAF). Individual mean alpha power (IAP) across TR epochs was also calculated. The alpha power timecourses were averaged across the six channels, mean subtracted and then normalised by the maximum power to control for differences between subjects.

In each subject we further identified two components which represented eye-blinks (EB) and eye-movements (EM), comparable to previous reports (Gao et al., 2010; Jung et al., 2000; Plochl et al., 2012). These were easily identified from a very strong central (EB) or dipolar, lateralized (EM) frontal topography and transient spikes (EB) or smoother power fluctuations (EM) of activity in the EEG timeseries (Figure S2). The clear identification of eye blink components throughout every subject's data provides evidence that none of our subjects fell asleep during the scan. The effect of eye movements on resting alpha-BOLD correlations has been sparsely investigated to-date therefore we quantified both EB and EM effects from the EEG to enable us to study whether alpha power or alpha-BOLD coupling were modulated by either eye movements or eye blinks. A timeseries of both EB and EM power was derived by taking the absolute value of the Hilbert envelope

of the EB and EM IC in each subject, the mean power of each TR epoch was then calculated to construct a regressor for subsequent fMRI analysis.

fMRI data preprocessing

All fMRI analyses were carried out using FSL 5.0 (www.fmrib.ox.ac.uk/fsl). Prior to statistical analysis, automated brain extraction using BET and motion correction using MCFLIRT (Jenkinson et al., 2002) were applied. At this point, two subjects were removed from further analysis due to excessive (>3mm) head motion. Physiological noise correction, using the standard RETROICOR procedure of linear regression (Glover et al., 2000) was then implemented using in-house MATLAB code. Subsequently, spatial smoothing (5 mm FWHM Gaussian kernel), high-pass temporal filtering (100s cutoff) and registration to high-resolution anatomical and MNI standard brain images were performed.

fMRI GLM analysis

GLM analysis was performed to identify the brain regions with significant static correlations between the entire BOLD signal and the entire alpha power timeseries. For each subject, first-level design matrices were formed from nine regressors: 1) the alpha power timecourse convolved with the canonical double-gamma haemodynamic response function; 2) respiration volume per unit time (RVT) (Birn et al., 2008); 3) variation in the heart-rate interval (HRI) (Chang et al., 2009); 4-9) six motion parameters of head translation and rotation. None of the regressors were orthogonalized with respect to any

other regressors as recommended by previous work (Chang et al., 2009; Chang and Glover, 2009; de Munck et al., 2009).

The RVT and HRI were calculated from the physiological data to control for potential differences in heart-rate and depth of respiration throughout the experiment. Previous work has reported a relationship between alpha and physiological variability (de Munck et al., 2008; Yuan et al., 2013). Modelling fluctuations in RVT and HRI with the GLM allows us to account for BOLD signal variability that is unrelated to neuronal activity, and removing these potential confounds will improve our estimate of the alpha-BOLD relationship.

First-level statistical analyses were performed using FEAT 6.01. Positive and negative contrasts were set on all regressors. Second-level, fixed-effects analysis was used to calculate the group average of static alpha-BOLD correlation maps. Additional group-level regressors were specified in the fixed-effects analysis, formed from individual variability in: 1) the IAF; 2) IAP, to investigate whether the strength of subject's alpha-BOLD correlation was related to basic characteristics of their alpha oscillation. All Z-statistic images were thresholded using clusters determined by $Z>2.3$ and a cluster corrected significance threshold of $p<0.05$.

Two additional GLM analyses were performed including the timeseries of EB and EM as regressors to investigate respectively the brain regions where BOLD signal correlated with eye-blinks and eye-movements as defined from the EEG data.

Definition of fMRI ICNs

BOLD data were temporally concatenated across subjects and MELODIC (Beckmann and Smith, 2004) was used to decompose this group data into 20 maximally spatially-independent components. From these components seven ICNs were identified by visual inspection: 1) default mode (DMN); 2) dorsal attention (DAN) 3) saliency (SAL); 4) sensorimotor (SM); 5) auditory (AD); 6) primary visual (PV) and 7) lateral visual (LV) networks (Figure S3). The primary nodes of each ICN were used to define regions of interest (ROIs) from these component maps, following previous work (Khalsa et al., 2013; Przezdzik et al., 2013). DMN: posterior cingulate (PCC), medial prefrontal cortex (mPFC); DAN: left intra-parietal sulcus (IPS) and lateral orbitofrontal cortex (OFC); SAL: left insula and anterior cingulate (ACC). The sensory ICNs (SM, AD, PV, LV) were divided into left and right hemisphere ROIs. All ROIs were defined by centering a 3x3x3 voxel cube (12x12x16mm) on the peak z-statistic voxel, located centrally in each region. Anatomical masks (Harvard-Oxford subcortical atlas, FSLatlas tools) were used to define an MNI-space ROI for the bilateral thalamus.

Characterizing dynamic alpha-BOLD relationships

The BOLD data were further processed to remove the trends of RVT and HRI using linear regression along with the mean white matter and ventricular signals were extracted from subject specific masks defined from each subject's T1-weighted anatomical image using FAST (Zhang et al., 2001). For each subject, the mean BOLD timecourse across voxels was then extracted from each ROI.

For each subject, the 6-minute alpha power timecourse was convolved with the canonical HRF to account for the haemodynamic delay and then divided into short epochs for dynamic analysis. The choice of window length is crucial, as previous work has shown results are strongly dependent on data length (Keilholz et al., 2013; Shakil et al., 2016; Wilson et al., 2015), see (Hindriks et al., 2016; Hutchison et al., 2013a; Leonardi and Van De Ville, 2015; Shakil et al., 2016) for excellent guidelines on dynamic analysis. Our choice of epoch length was guided by previous studies of dynamic fMRI functional connectivity, the majority of which used windows in the range 30-120s (Allen et al., 2014; Betzel et al., 2016; Chang and Glover, 2010; Chang et al., 2013; Gonzalez-Castillo et al., 2014; Hutchison et al., 2013a; Hutchison et al., 2013b; Keilholz et al., 2013; Kiviniemi et al., 2011; Leonardi and Van De Ville, 2015; Shakil et al., 2016; Tagliazucchi et al., 2012; Thompson et al., 2013a; Thompson et al., 2013b; Wilson et al., 2015; Yu et al., 2016; Zalesky et al., 2014) but lower bounds of 12s and 16s are also described (Shakil et al., 2016; Thompson et al., 2013a; Wilson et al., 2015). Dynamic measures are limited by the inescapable trade-off that increasing temporal resolution comes at the cost of a decrease in the fidelity of correlations calculated over fewer time points. Appropriate window size is related to the frequency content of the data as the lowest frequency content of the signal dictates the minimum window size. A previous investigation identified appropriate FC epoch lengths based on the data properties (Leonardi and Van De Ville, 2015). For the filtering used in the present study their criteria recommend that we use epoch lengths between 12-60s. Therefore to conform with this, to provide comparison with previous work and to obtain the best possible temporal resolution to study variations in alpha power, we use

four subsets of epochs of duration: 60s, 32s, 16s, 8s (30, 16, 8, 4 TRs respectively) with a 50% overlap, resulting in 11, 21, 44, 89 epochs per subject respectively. The timeseries of each of these alpha power epochs was then correlated with the corresponding temporal epoch of the BOLD data from each brain voxel, creating a sliding window correlation analysis to characterise the temporal dynamics of the alpha-BOLD relationship across the whole brain. This approach is analogous to many previous studies of dynamic functional connectivity (Handwerker et al., 2012; Hindriks et al., 2016; Hutchison et al., 2013b; Keilholz et al., 2013; Shakil et al., 2016; Wilson et al., 2015) but here we use EEG alpha power instead of a seed BOLD timecourse. For each epoch, a voxel-wise map of Pearson's R-values was created. Each epoch R-value map was masked with each ICN ROI to extract the mean R-value per ROI which resulted in a timeseries of R-values characterising the temporal dynamics of the alpha-BOLD relationship for each ROI. For each subject and each ROI, the static correlation between the whole 6-minute timeseries of BOLD signal and alpha power was also calculated.

We evaluated our measures of dynamic alpha-BOLD correlation for each ROI in three ways: 1) by comparing the group mean regional static correlation strength (R-value) to the group mean dynamic correlation for each of the four epoch durations. A repeated measures ANOVA (Factors: Epoch (Static,60s,32s,16s,8s) x ROI) was used to test for a significant difference in R-value between static and dynamic correlation methods; 2) for each ROI, the subject's static alpha-BOLD correlation strength was correlated against their mean number of epochs that exhibited a positive or a negative alpha-BOLD correlation; 3) For display purposes volumetric maps of the alpha-BOLD correlation were transformed to Z-statistics and averaged across epochs for each subject. Group

mean statistical maps were then calculated using random effects 2nd level analysis ($p<0.001$ uncorrected) in SPM8 (www.fil.ion.ucl.ac.uk/spm/).

At this point, from the options considered the 16s epoch duration was identified as providing the most preferable combination of increased temporal resolution and robust measurement of the alpha-BOLD relationship (see Results). It isn't feasible to concisely present a detailed study of the many features of alpha-BOLD dynamics for all window lengths so for brevity we used 16s epochs for all subsequent analyses. The timecourse of total relative movement, obtained from MCFLIRT as a summary parameter of each subject's head motion, was used to calculate the correlation between alpha power and head motion for each 16s epoch. Epochs with a significant ($p<0.05$) alpha-motion correlation were removed from further analysis. On average, 4.1±1.6 out of 44 epochs (range 1 to 7) were removed which ensured that dynamic alpha-BOLD correlation measurements are minimally confounded by artefacts or noise.

Proportion and distribution of dynamic alpha-BOLD correlations

For each ROI we assessed the frequency of alpha-BOLD correlation strength for each subject, and then calculated the group mean proportion of epochs that showed: a) positive or negative correlations ($R > 0$ or $R < 0$); b) or strong correlations ($R > 0.5$ or $R < -0.5$.). These data were plotted as group histograms to visualize the distribution of dynamic correlations across all subjects.

We wished to understand how often the spatial pattern of dynamic alpha-BOLD correlations resembled the static correlation network and how often it passed through

different spatial configurations. Therefore we compare the proportion of the time that the spatial pattern of dynamic alpha-BOLD correlations reflects that of the static correlation (i.e. negative correlation with visual areas and the DAN occurring concurrently with a positive correlation with the DMN and thalamus) compared to how often the dynamic correlations reflect the inverse of the static correlation (positive alpha-visual/DAN or negative alpha-DMN/thalamus correlations). Therefore we calculated the proportion of epochs during which the BOLD signals of the PV, LV and IPS ROIs were all negatively correlated with alpha power whilst BOLD signals in the PCC and THL were positively correlated with alpha. We further calculated what proportion of the time alpha was correlated only with different sub-regions of this network, such as just PV and LV. These comparisons informed us about the combinations of regional correlations, and the extent to which the regions that exhibited a negative, static BOLD-alpha correlation on average (i.e. PV, LV, DAN) are uncoupled from alpha power (and by extension uncoupled from each other) on a shorter temporal scale. Finally we demonstrate some representative examples of the unusual configurations that the spatial patterns of alpha-BOLD correlations can take. For each subject we found the epochs where the following correlations, which diverged from the static behavior, were observed: (A) positive alpha-BOLD correlations with LV, (B) positive with PV, (C) negative with THAL and (D) negative with PCC. All subjects contributed epochs to the group averages showing that these configurations were consistent across the group. For each example, we pooled the epochs across subjects and calculated group mean maps of voxel-wise alpha-BOLD correlations using random effects 2nd level analysis ($p<0.001$ uncorrected) in SPM8 (www.fil.ion.ucl.ac.uk/spm/)..

.

Investigating the effect of dynamic alpha power on alpha-ICN correlations

We finally investigated whether the strength of the regional alpha-BOLD correlation varied with temporal fluctuations in alpha power within the session. Within each subject, epochs were ranked by their alpha power to enable comparison of alpha-BOLD relationships between periods where alpha power was low compared to high. Firstly, for each subject the proportion of epochs with alpha power above and below the mean value was calculated. Secondly, for each ROI, the epoch R-values of alpha-BOLD correlation were sorted into two subgroups; the epochs with the highest and lowest thirds of alpha power respectively. Thirds were chosen, rather than a median split, because of the uneven distribution of alpha power across epochs (see Figure S6) and all subjects had at least 33% of epochs with power greater than the mean value. A repeated measures ANOVA (Factors: ROI x Power (Lower, Upper)) was used to test for a significant effect of alpha power upon the alpha-BOLD correlation strength. Where appropriate (i.e. only if a significant main effect or interaction was observed) post-hoc t-tests were used to compare correlation values between lower and upper alpha power within each ROI. Thirdly, to visualize differences in the spatial pattern of alpha-BOLD correlations between low and high alpha power epochs across the whole brain, the voxel-wise maps of alpha-BOLD correlation were sorted into lower and upper thirds based on the corresponding epochs alpha power and then averaged for each subject. Group mean statistical maps of alpha-BOLD correlations for upper and lower alpha thirds were then calculated using random effects 2^{nd} level analysis ($p<0.001$ uncorrected) in SPM8.

Investigating the relationship between dynamic alpha-BOLD correlations and single-trial BOLD responses to stimulation.

An additional EEG-fMRI dataset was used to investigate whether the temporal dynamics of the alpha-BOLD correlation relate to the magnitude of the brains response to subsequent visual stimulation. Full experimental details can be found in (Ostwald et al., 2010; Porcaro et al., 2010) but briefly in 14 healthy young adult subjects, 85 100%-contrast left-hemifield checkerboard visual stimuli were displayed for 2s separated by an interval between 16.5-20s. 64-channel EEG data were recorded simultaneously with BOLD fMRI data at 3T, TR = 1500ms, TE = 35ms, 2.5 x 2.5 x 3mm voxels, 20 slices centered on visual cortex. The timecourse of ongoing alpha power was extracted using equivalent ICA methods to those described above and convolved with the canonical HRF. BOLD data were standardly preprocessed and the ICN ROIs employed above were registered to this task data along with the right primary visual cortex (rV1) ROI of significant BOLD response to the visual stimulation described in (Mayhew et al., 2013b). Single-trial BOLD response timecourses were extracted from the rV1 ROI and their peak amplitudes measured. Trials were then sorted into lower and upper 25% quartiles of response amplitude and we compared the spatiotemporal profile of alpha-BOLD correlations between these largest and smallest BOLD responses.

Dynamic, voxel-wise alpha-BOLD correlation maps were then calculated in this task data using a series of 13.5s (9 TR) duration epochs centered on every volume of the dataset. For each trial, a 4D volumetric timeseries was created from the nine most temporally

local epochs, centered on TR = -4,-3,-2,-1,0,1,2,3,4 relative to the stimulus onset, therefore encompassing the period -12s preceding to +12s following stimulation. This formed a timeseries of alpha-BOLD correlation maps that enabled us to track the regional variation in alpha-BOLD dynamics from pre- to peri- and post-stimulus time points. These correlation map timeseries were arranged into quartiles corresponding to the trials with lower and upper 25% of BOLD response amplitude. The rV1 ROI, along with a combined visual cortex ROI (PV and LV) as well as the IPS and INS ROIs were then used to extract mean alpha-BOLD correlations for each of the nine epochs and for both quartiles. A repeated measures ANOVA (factors: BOLD quartile x Epoch) was used to test for significant differences in alpha-BOLD correlation in each ROI. For display purposes group mean statistical maps of alpha-BOLD correlations for upper and lower BOLD response quartiles, as well as significant voxel-wise differences between them, were then calculated using random effects 2nd level analysis ($p<0.001$ uncorrected) in SPM8.

Results

Static alpha-BOLD correlations

Figure 1A displays the group GLM results of the brain regions where the resting-state BOLD signal was significantly correlated with the whole 6-minute alpha power timecourse. In agreement with previous reports we found significant static alpha-BOLD positive correlations in the bilateral thalamus and the DMN, as well as significant static negative correlations in bilateral primary and lateral visual regions, the DAN and small

areas of the insula cortex (de Munck et al., 2007; Goldman et al., 2002; Laufs et al., 2006; Liu et al., 2012; Mo et al., 2012; Moosmann et al., 2003; Zhan et al., 2014). Modelling variations in the depth of the subject's breathing (RVT) and cardiac rate (HRI) as confounds of no interest in the GLM showed that BOLD responses were significantly correlated with these physiological fluctuations in widespread areas of grey matter in agreement with previous work (Figure S4) (Birn et al., 2008; Chang et al., 2009).

Inspection of first-level statistical maps revealed that all subjects showed at least one regional alpha-BOLD correlation comparable in polarity to the spatial map of group-level static correlation, but also highlighted between-subject variability in alpha-BOLD correlations (Goncalves et al., 2006). For instance, four subjects exhibited no significant negative alpha-BOLD correlation in any visual region. Six subjects showed a negative alpha-BOLD correlation in primary visual but not lateral visual regions and seven subjects showed negative alpha-BOLD correlation in lateral but not primary visual regions. These results indicate the between-subject variability in static alpha-BOLD correlations.

Group GLM analysis revealed a significant positive relationship between the negative alpha-BOLD correlation and the between-subject variability in the IAP, predominantly in occipital and parietal cortex (Figure 1B). In addition a significant negative relationship between the negative alpha-BOLD correlation and the between-subject variability in the IAF was seen mainly in occipital, parietal and insula cortex (Figure 1C). We observed no correlation ($R=-0.24$, $p=0.21$) between IAF and IAP measures indicating that these explain different components of between-subject variance in the data. These correlations can be interpreted as showing that subjects with lower IAF, or higher IAP, exhibited

stronger magnitude negative alpha-BOLD correlations in the identified brain areas. Both IAP and IAF correlations were widespread in primary and lateral visual cortex. The largest spatial differences between IAP and IAF were observed outside of visual regions, with IAF explaining alpha-BOLD correlation strength in the insula, the lateral geniculate nucleus (LGN), and anterior IPS regions of the DAN, compared to IAP showing stronger correlations in posterior IPS (Figure 1C). No significant between-subject variation with either IAP or IAF was observed in positive alpha-BOLD correlation regions of the thalamus and DMN.

Dynamic alpha-BOLD correlations during the resting-state

The group mean spatial correlation between the static and dynamic (TR) scalp topographies of alpha power was R= 0.65 ± 0.06, showing that in general the spatial distribution of alpha was temporally consistent and closely resembled the average. Henceforth we assumed the occipito-parietal alpha source to be spatially static and investigated the temporal variability of regional alpha-BOLD relationships using dynamic correlations calculated over short temporal windows of either: 60, 32, 16 or 8s. For each ROI, the strength and sign of the alpha-BOLD correlation were highly comparable between the static value and the dynamic epoch calculations down to windows as short as 16s (Figure 2A). The 8s correlation shows a substantial drop in correlation strength compared to the other epoch lengths (41% compared to 16s), demonstrating a decrease in the fidelity of the measured correlation for epochs containing very few timepoints. All subsequent results are presented using the more robust 16s

epoch length. It should be noted that we do not attach any special relevance or advantage to 16s epoch specifically, but just wish to investigate alpha-BOLD dynamics with a good trade-off between temporal resolution and signal to noise ratio. Repeated measures ANOVA found a significant effect of ROI ($F(4.3,117) = 10.6$, $p=0.001$) as would be expected, but no significant effect of Epoch ($F(1.9,504) = 1.8$, $p=0.18$), or interaction between Epoch and ROI ($F(9,242) = 0.89$, $p=0.51$). Figure 2B shows the group mean voxel-wise map of dynamic alpha-BOLD correlations averaged across all 16s epochs. Dynamic alpha-BOLD correlations were negative in primary visual, lateral visual and DAN regions and positive in the thalamus and DMN, showing a very strong spatial similarity to the static correlations. This demonstrated that dynamic correlations accurately characterised the mean relationship, providing similar information to static correlations, but with greater temporal information. It is interesting to note that the variability in the alpha-BOLD correlation was largely consistent between regions, aside from the ACC where variability was lower, suggesting that correlation stability does not vary greatly across the brain.

In addition, for each ROI, we observed that the between-subjects variability in the static alpha-BOLD correlation was significantly correlated with the number of epochs displaying an alpha-BOLD correlation of a certain polarity (Figure S5) i.e. subjects with the largest magnitude negative static alpha-BOLD correlation had the largest number of negatively correlated alpha-BOLD epochs, and vice-versa. Together these results demonstrate that alpha-BOLD correlations can be calculated using short temporal windows of 16s (8 MR samples), revealing highly comparable values to those of static

correlations. Therefore we conclude that dynamic correlations extract information that enables more detailed study of the temporal fluctuations between alpha and BOLD.

Proportion and distribution of dynamic alpha-BOLD correlations

Measurement of dynamic alpha-BOLD correlations allows us to move forward from the simplistic assumption of a static, single-polarity, alpha-BOLD relationship and examine the frequency of individual regional relationships and also the proportion of time in which alpha power is correlated with the BOLD signal from different regions.

Figure 3 shows, for each ICN, the group mean proportion of epochs with a negative or positive correlation (A) or a strong negative or positive correlation (B), for group histograms see Figure S6. Surprisingly, no ROI showed a bias in correlation polarity greater than ~60/40% in favour of its group mean static correlation. PV was the ROI with largest disparity with 61% (39%) negative (positive) alpha-BOLD correlation epochs. LV (59/41%) and IPS (58/42%) showed more negatively than positively correlated epochs and THL (54/46%), and DMN (53/47%) regions more positive than negative epochs, but most regions showed only a small divergence from a 50/50% split (Fig 3A). Further analysis showed that 27% of epochs exhibited a strong ($R<-0.5$) negative PV-alpha correlation, however approximately half that amount (13%) showed a strong ($R>0.5$) positive PV-correlation (Fig 3B). For all ROIs the most common direction of dynamic correlation matched the polarity of the static correlation, as would be expected. However, surprisingly no ROI other that PV exhibited more than a quarter of epochs with a strong dynamic correlation of the same polarity as the static correlation.

Further analysis of dynamic correlation proportions is summarized in Table 1 and Figure 4. Figure 4 displays the group mean proportion of epochs during which the dynamic analysis detected the same alpha-BOLD correlation polarity as was demonstrated in the static analysis. The first six segments, moving clockwise (purple to grey) around the chart represent (in total) the 59% of the time when a negative PV-alpha correlation was observed. This total time is divided into subsections showing when, e.g. alpha was concurrently negatively correlated with PV, LV and IPS as well as positively correlated with PCC and THL (black). Whereas the time (45%) that both PV and LV were negatively correlated is represented by the first four segments (purple to cyan). The last three segments (yellow to red) represent the 41% of the time when positive PV-alpha correlations were observed, including 20% of the time when one of either LV or IPS was negatively correlated (yellow). Figure 4 further shows that 43% of the time, an opposite polarity alpha-BOLD correlation was observed between either PV&IPS or between PV&LV (light blue to yellow). Table 1 contains other interesting combinations of regional alpha-BOLD correlations, for example that either PV or LV were negatively correlated with BOLD 75.1% of the time.

In general, we observed that only 7.7% of epochs showed the same polarity of dynamic correlation as was shown in the static correlation (i.e. negative PV, LV&IPS and positive PCC&THL, Fig 1). However, the opposite situation hardly ever occurred, and it was also very rare for both PCC and THL to be negatively correlated with alpha at the same time as PV, LV and IPS. Only during 35% of epochs did we observe that all of the PV/LV/IPS ROIs were concurrently negatively correlated with alpha power. Approximately 44% of epochs showed a negative correlation with alpha between two ROIs out of PV/LV/IPS. In

approximately 10% of the total epochs one of those three ROIs was uncoupled from alpha.

Further demonstration that resting-state alpha-BOLD coupling adopts spatial configurations quite different from that of the static average is shown in Figure 5. We observed that during periods of positive alpha-LV correlation (Fig 5A), alpha was also positively coupled to bilateral auditory and sensorimotor cortex as well as the middle/anterior cingulate cortex but no correlation with primary visual areas was seen. The map during positive alpha-PV correlations (Fig 5B) was quite different, it also showed cingulate regions but no other sensory cortex. Instead weak positive alpha-BOLD coupling was seen in DMN regions. The map during negative alpha-THL correlations (Fig 5C) showed that alpha was also strongly negatively correlated with the whole visual cortex during these periods. Also observed in Fig 5C were correlations with PCC and mPFC DMN regions, and bilateral parietal and sensorimotor cortex. Finally, during epochs that exhibited negative alpha-PCC correlations (Fig 5D), negative correlations with the rest of the DMN were seen and the only other correlation was negative coupling between alpha and visual cortex.

Regional effect of dynamic alpha power on alpha-ICN correlations

We further investigated whether the instantaneous power of the alpha oscillation affected the temporal dynamics of the alpha-BOLD correlation in a regionally dependent manner. For all subjects, we found that a larger proportion of epochs exhibited alpha power values that were less than the mean within-run value (58.9±4.3% of epochs, group mean ± std)

than were greater than the mean 41.1±4.2% (Figure S7). This result shows that the alpha oscillation is more commonly found in a weakly-synchronised than a highly-synchronised state during awake rest. These findings are in accordance with descriptions and models of the non-linear nature of the alpha oscillation and that longer periods of quiescent, low power are intrinsically interspersed with transient bursts of high power (Freyer et al., 2009).

Figure 6A compares the group mean dynamic correlation for each ROI between epochs with the lowest and highest third of alpha power values. We observed that the regional alpha-BOLD correlation displayed a dependency upon alpha power. Repeated measures ANOVA showed a significant effect of Power ($F(1,27)=4.5$, $p=0.016$), ROI ($F(4.9,132)=4.9$, $p=0.001$) and a significant interaction between Power x ROI ($F(4.3,118)=6.2$, $p=0.008$). Selective post-hoc student's t-tests were subsequently used to highlight the ROIs contributing to this interaction effect. This showed that PV-alpha, INS-alpha and ACC-alpha correlations were significantly more negative ($p=0.004$, $p=0.007$ and $p=0.002$ respectively during low than during high alpha power epochs, which remain below the 0.05 significance threshold after correcting for multiple (seven) comparisons). Additionally, it was notable that during the epochs of lowest alpha power, the alpha-BOLD correlation in PV was not significantly different from zero ($p=0.64$), whereas in the epochs of highest alpha power the PV-BOLD correlation was strongly negative. The largest difference in correlation between upper and lower alpha power epochs was observed in the INS and ACC regions of the saliency network, where the alpha-BOLD correlation was positive in lower epochs, and negative in the upper epochs. This strong dependence of saliency-alpha correlations upon alpha power suggests the

presence of a high-degree to temporal variability which may explain why this network is only weakly correlated with alpha in static correlations (Figure 1).

In contrast, IPS-alpha and LV-alpha correlations were more negative during epochs when alpha power was low than epochs when it was high, although neither of these reached significance ($p=0.18$ and $p=0.09$ respectively). Alpha correlations with the DMN were significantly more positive in the mPFC when alpha power was low compared to high ($p=0.03$). Alpha correlations with THL were also more positive when alpha power was low compared to high ($p=0.04$).

Further elucidation of these findings is provided by the group mean spatial maps of voxel-wise alpha-BOLD correlations plotted for both the highest and lowest alpha power epochs in Figure 6B&C. The lower alpha power epochs showed a greater spatial extent of negative alpha-BOLD correlation in both LV and IPS areas whereas PV-alpha and INS-alpha correlations were much stronger and more widespread in higher alpha power epochs. Also evident were widespread negative alpha-BOLD correlations in secondary somatosensory regions during low alpha power epochs and in subcortical LGN and brainstem areas during high alpha power epochs. The conjunction of areas of alpha-BOLD correlation that occurred in both lower and upper alpha power epochs was most prevalent in the DAN, particularly the anterior regions. A positive alpha-BOLD correlation in the thalamus, the ACC and the DMN was only observed in lower alpha power epochs.

The relationship between the BOLD signal and spontaneous eye-blinks and eye–movements

Additional GLM analyses showed that the power of eye-blinks derived from ICA of the EEG data correlated positively with the BOLD signal in PV, the cuneus, the LGN and mid-THL; and negatively with the BOLD signal in LV and in the parietal and inferior and medial frontal regions of the DAN (Figure 7A&B). In comparison the power of eye movements were found to only correlate positively with BOLD signal in PV, the cuneus, the LGN and mid-thalamus as well as widespread cortical regions consisting of anterior cingulate, bilateral insula, parietal and frontal eye-field regions (Figure 7C). This relationship can be interpreted as showing that larger EB and EM are associated with increased BOLD signal in primary visual, thalamic and fronto-parietal areas showing our novel EEG derived metrics are consistent with previous work using eye tracking (Bristow et al., 2005; Guipponi et al., 2014; Hupe et al., 2012). Interestingly the inclusion of the EB and EM regressors in the GLM only slightly weakened the statistics of the main effect static alpha-BOLD correlation [peak Z-statistic = 13.6 (without EB/EM); Z = 13.3 (with EB/EM)] demonstrating a large degree of orthogonality between the BOLD signal correlates of ocular artefacts and alpha power.

We compared the occurrence of eye blinks and movements with dynamic epoch measurements of alpha power by correlating measures of alpha power with EB and EM calculated over equivalent 16s duration epochs. A significant relationship between either EB-alpha or EM-alpha was found in only 3 and 4 subjects respectively, suggesting that our dynamic measurement of alpha-power reflects spontaneous fluctuations in the

neuronal signal and is predominantly independent of modulations driven by eye movements and closures.

The relationship between dynamic alpha-BOLD correlations and single-trial BOLD responses to stimulation

To illustrate the wider utility and functional importance of the dynamic alpha-BOLD correlation approach presented above, we applied the method to relate pre-, peri and post-stimulus temporal variations in alpha-BOLD correlations to the magnitude of the brains response to a simple visual stimulus. Figure 8 illustrates the temporal profile of alpha-BOLD correlations in rV1, bilateral PV+LV, IPS and INS ROIs for lower and upper quartiles of the rV1 BOLD response to stimulation. It should be noted that only the first and last points fully capture the pre- and post-stimulus time window.

We found that the large difference in BOLD response amplitude between trial quartiles was associated with significant pre-stimulus and post-stimulus differences in the strength and spatial extent of alpha-BOLD correlation in visual cortex regions (Figure 8A&B). Repeated measures ANOVA found a significant effect of Sorting and of Epoch upon the alpha-BOLD correlations for both rV1 ($F(1,9)=7.9$, $p=0.02$); ($F(8,72)=5.2$, $p=0.01$) and PV+LV ($F(1,9)=6.4$, $p=0.03$); ($F(8,72)=4.8$, $p=0.02$) regions respectively. No significant interaction was observed or any significant effects for the IPS or INS regions.

As shown in Figure 8, negative alpha-BOLD correlation in visual cortex was stronger for upper than lower quartile responses throughout. However, two distinct temporal phases were observed. High BOLD response trials had significantly stronger alpha-BOLD

correlations pre-stimulus and during the post-stimulus response period. The temporal profile during high response trials shows that the alpha-BOLD correlation was strongly negative at -6s prestimulus, it then weakened in the lead up to immediately prestimulus time points but then greatly increased in strength during the response period. In comparison the low response trials show signs of strengthening alpha-BOLD correlation immediately prestimulus which then weakens during the response period. At 6s, around the time of the BOLD response peak, alpha-BOLD correlations attain comparable strengths between upper and lower response trials. Alpha-BOLD coupling strengths for the two quartiles appear to converge in the period immediately prestimulus, but after stimulation the coupling changes in opposite directions such that for the lowest response trials almost no alpha-BOLD correlation is observed in visual cortex at 0-1.5s. The maps at the top of the figure further illustrate how the spatial pattern of alpha-BOLD correlations evolved over time for trials with very different BOLD response amplitudes and the regions with significant differences in coupling between lower and upper response quartiles.

Discussion

This study demonstrates that considerable within- and between-subject variability exists in the spatiotemporal pattern of alpha-BOLD correlations in the human brain during eyes-open rest. We show that alpha-BOLD correlations can be accurately measured using 16s sliding window epochs, and use this increased temporal resolution to show how the alpha-BOLD correlation in distinct ICNs fluctuates over time, varies between ICNs and

shows a complex relationship with alpha power amplitude. In general we find that the general assumption of a static, inverse alpha-BOLD relationship is a considerable oversimplification and that the static network is fully coherent during only a small proportion of the total experiment time. Our results suggest that the static network does not fluctuate coherently as a whole entity in its correlation with alpha power. Instead of periodically waxing and waning in strength the static network loses its coherence such that its different regional components correlate with alpha during different periods of time.

By correcting for physiological noise, head-motion and accounting for eye movement/blink events, we have taken thorough steps to remove their potential confounding effects upon temporal fluctuations in alpha-BOLD correlations, and demonstrated that they are not driving the results that we observe. Additionally, we find that the trial-by-trial amplitude of V1 BOLD responses to visual stimulation could be predicted by the strength of the alpha-BOLD correlation in the visual cortex, demonstrating the utility of sliding window alpha-BOLD analysis to provide functional information about brain dynamics.

Between-subject variability in static correlations

Individuals with the highest alpha power and lowest alpha frequency exhibited the strongest, static alpha-BOLD negative correlations (Fig1B&C). These results indicate that between-subject variability in mean alpha properties has metabolic consequences which can be detected as differences in alpha-BOLD coupling, which is consistent with

previous reports that oscillation power and frequency reflect bulk neurophysiological characteristics of an individual that are stable over sessions (Kondacs and Szabo, 1999; Napflin et al., 2007), related to cortical volume (Schwarzkopf et al., 2012), white matter connections (Hindriks et al., 2015) and even genetic factors (Bodenmann et al., 2009). In addition our results inversely linking the frequency of alpha to the strength and spatial extent of its correlation with the BOLD signal suggest that oscillation frequency may inform about the activity and size of the underlying generating neuronal network given that lower frequency alpha oscillations represent synchronous activity over a larger cortical network (Grandy et al., 2013; Koch et al., 2008; Kondacs and Szabo, 1999; Singer, 1993; Varela et al., 2001) which encompasses greater total neuronal activity and stronger BOLD signal (Fig 1B&C). It is well known that IAP varies substantially between subjects, which is why normalization is often used in group analyses, and here we show that the subjects with the strongest IAP show the strongest alpha-BOLD coupling over occipito-parietal regions. However until an improved understanding of the origin of inter-individual differences in alpha oscillations, including the contributions of current source orientation, cortical volume, brain geometry and skull thickness or the signal-to-noise ratio of the EEG measurement (which would be affected by the efficacy of MR artifact correction) is obtained, the functional interpretation of these effects remains obscure.

Spatiotemporal, within-subject variability in alpha-BOLD coupling.

Fluctuations in alpha power were not consistently correlated with the BOLD signal during the resting-state, instead we observed spatiotemporal variations in correlation structure as alpha-BOLD coupling occurred in different sub-components of the static "network" as a function of time. Overall, the brain regions which demonstrated static correlations (Fig 1) appeared to represent the mean spatial network that would be formed by averaging together the distinct, power-dependent patterns of dynamic correlations. In an additional task EEG-fMRI dataset we found that dynamic alpha-BOLD correlations exhibited temporal and spatial variations related to the magnitude of the BOLD response to visual stimulation, showing that this coupling can also provide functional information pertaining to the brain's response to experimental tasks.

All investigated brain regions showed substantial variability in not only the strength of the resting-state alpha-BOLD correlation, but also its polarity (Figs 3,4,5,6). Many regions showed an approximately even division between the time spent demonstrating positive or negative correlations. Even primary visual cortex, the region which exhibited the strongest negative correlation with alpha, was positively correlated with alpha during 40% of epochs on average and very strongly positively correlated with alpha during 15% of epochs.

In addition to finding that alpha-BOLD correlations were highly dynamic within-ROI, we also found considerable variability between-ROIs. For instance, during only 8% of the total time did the dynamic correlations reproduce the entire network observed in the static correlation map (Table 1 and Fig 4). Furthermore, during only 36% of epochs were all three of the regions which dominated the static correlations (PV, LV and IPS) concurrently negatively correlated with alpha power. It was also quite common for

multiple regions of the static correlation network to concurrently display opposite correlations with alpha power. We even observed this dissociation between primary and lateral visual cortex, as only 45% of the time were both visual ROIs correlated negatively with alpha. Visualising the voxel-wise maps of the more unusual alpha-BOLD coupling patterns showed some unique associations, such as periods during which the alpha correlation with both PV and THL (or both PV and DMN) had the same polarity (Fig 5B-D), in contrast to opposite polarity in static measures. We also observed a multi-sensory state where LV, auditory and sensorimotor cortex were all positively coupled to alpha power at times when PV was uncorrelated.

This dynamic behavior of alpha-BOLD coupling doubtless reflects the intrinsic temporal fluctuations in, and the hierarchical organisation of, brain network connectivity. What we observe here are some examples of the many configurations of the activity patterns that the brain passes through during the unconstrained resting-state, ranging from the largely temporally distinct fluctuations of signals from different ICNs, to the partial separation observed between subcomponents of the whole visual network. These varying configurations are associated with switching between vigilance states, internal/external thought and memory processes and general mind-wandering alongside temporal fluctuations in the power of the alpha oscillation. Links between variability of ICN and electrophysiological activity are beginning to be studied (Betti et al., 2013; Brookes et al., 2011; Chang et al., 2013; Mantini et al., 2007; Vincent et al., 2007) and identification of the processes that could give rise to variations in alpha-BOLD coupling over time is an important topic for future work aiming to understand the functional significance of distinct patterns in within- and between-ICN connectivity.

Alpha sources and the variation of alpha-BOLD coupling with alpha power.

The present study assumes a single, static spatial source of alpha activity, which although we found a high degree of similarity between the dynamic and the static topographies, is likely an oversimplification. Posterior alpha can be locally generated in V1 (Bollimunta et al., 2008) and via bottom-up, pacemaking drive from the thalamus (Hughes and Crunelli, 2005; Lopes da Silva, 1991) which dominates during rest (Goldman et al., 2002; Roux et al., 2013), although it is likely that modulations also occur due to spontaneous recruitment of top-down feedback influences (von Stein et al., 2000) primarily from higher order areas such as the DAN (Bastos et al., 2015; Capotosto et al., 2009; van Kerkoerle et al., 2014) but potentially also the PCC, INS/ACC as these regions display alpha-BOLD correlations by association even though they are not thought to directly contribute to posterior alpha generation. Future work needs to further elucidate multiple alpha sources and their relationship with dynamic patterns of alpha-BOLD coupling

Dynamic alpha-BOLD coupling displays a complex range of configuration patterns which argue against a simple periodic waxing and waning in the coherence of the whole static network's activity with the amplitude of alpha power (or measurement SNR). If regional dissociation of alpha-BOLD coupling (e.g. as seen between PV and LV) were simply due to fluctuations in the prominence of activity between two separate alpha sources, such that the activity of one source reduced as the other concurrently increased, then due to volume conduction overall posterior EEG alpha power would be consistent

between both states. Although such a scenario could explain variations in the spatial location of the strongest alpha-BOLD correlation over time, no clear relationship between alpha-BOLD coupling and alpha power would be observed. In contrast, our data shows that the spatiotemporal dynamics of resting alpha-BOLD coupling depended on the epoch's level of alpha power, and that PV and LV were most strongly negatively correlated with alpha during different alpha power states. The strong alpha-BOLD coupling observed in PV during high alpha power is consistent with evidence that PV acts as a cortical alpha generator (Bollimunta et al., 2011; Buffalo et al., 2011). The surprising finding was that LV regions were often uncoupled from PV during high alpha power and that during low alpha power we observed a different spatial pattern of alpha-BOLD correlation, rather than a weaker version of the same network. Therefore temporal fluctuations in alpha-BOLD coupling of the static network did not appear to neatly align with the magnitude of alpha power.

Alpha-BOLD coupling during stimulation - relationship between changes in brain metabolism and oscillation synchrony.

In the task EEG-fMRI recording we found that alpha-BOLD coupling was largely coherent between PV and LV regions but its strength varied between pre- and post-stimulus time points in relation to the amplitude of the visual cortex BOLD response to stimulation (Fig 8E). A state of low alpha-BOLD correlation in the visual cortex preceding stimulation was predictive of a small amplitude V1 response and further reduced alpha-BOLD coupling post-stimulation, whereas in high response trials a

strongly negative alpha-BOLD correlation pre-stimulus was followed by a large V1 BOLD response and stronger alpha-BOLD coupling post-stimulation. When interpreting the spatial variation in these results it must be considered that the alpha-BOLD is likely to depend on the SNR of both signals, which could explain why the regions with the strongest responses (PV and LV) show the greatest effect. The alpha oscillation was desynchronized by the visual stimulus (Mayhew et al., 2013b) but this brief (2s) duration effect was not correlated with the BOLD amplitude and therefore differences in alpha response are unlikely to give rise to the BOLD variability observed. Our previous work showed that 500ms prestimulus alpha power was inversely related to the amplitude of the subsequent BOLD response but predominantly in negative BOLD regions with only a small effect on the positive BOLD response in anterior V1 (Mayhew et al., 2013b) in comparison to the more widespread visual effect seen with alpha-BOLD coupling. Taken together these results indicate that the magnitude of the BOLD response is strongly linked to alpha-BOLD coupling and suggest that visual cortex BOLD responses depend on several features of preceding brain activity. This finding is in agreement with previous neuroimaging studies which showed that the brain's responsiveness to a stimulus can be predicted by activity measures obtained from the pre-stimulus resting state (Boly et al., 2007; Eichele et al., 2008; Sadaghiani et al., 2009; Sadaghiani et al., 2015).

Variations in the BOLD response amplitude to a consistent stimulus input likely reflect a combination of temporal drifts in subject's attention, alertness and quality of fixation as well as spontaneous fluctuations in the excitability of the underlying neural network. The largest response trials occur when a more responsive, coherent cortical system arises from a mutual alignment of these factors. We suggest that a tight coupling between alpha

power and BOLD in visual cortex, independent of the level of alpha power, reflects synchronised activity in a network that is primed to respond. Consequently, following such a state, a large BOLD response to stimulation and strong alpha-BOLD coupling is observed. When interpreting EEG-BOLD correlations it must be remembered that no single frequency band can alone be expected to explain BOLD signal variance, which represents an integration of the metabolic demand of broadband activity and appears most strongly correlated with gamma (>40Hz) frequencies (Logothetis, 2002; Magri et al., 2012; Scheeringa et al., 2011a). In addition, the influence of other ICNs such as the DMN can also to explain variance in stimulus responses (Mayhew et al., 2013a).

Potential and possible confounds in dynamic analyses

Dynamic analyses based on sliding, short-duration windows offer advantages for assessing the relationship between simultaneously recorded EEG-BOLD signals. However, as with any study involving short time window measures, there is the risk of contamination by noise and also the inherent difficulty in evaluating whether temporal fluctuations in correlation can be taken as evidence of the presence of dynamic functional relationships (Hindriks et al., 2016). For fMRI data, with a TR typically on the order of seconds, shortening time windows will always come at the cost of reducing the signal-to-noise ratio of the measure and therefore, although potentially providing more functional information, are subject to statistical uncertainty as the dynamic measures are only estimates of the true underlying, unknown, correlation. Determining the accuracy of dynamic measures is challenging without a detailed understanding of the signals

constituent noise sources, although see (Chang et al., 2013; Handwerker et al., 2012; Hindriks et al., 2016; Keilholz et al., 2013; Zalesky et al., 2014) for suggested test statistics.

Here we cite the similarity between the correlation values of the static and the mean 16s, 32 and 60s epoch as suggesting dynamic analysis provides a meaningful measure of temporal fluctuations in alpha-BOLD coupling. Whilst this does not constitute an unambiguous validation, if epochs were substantially confounded by noise it would be expected that the average correlation would approach zero, which we did not observe as a fall-off in signal was only found for 8s epochs. We have used a similar approach for examining dynamic functional connectivity previously (Wilson et al., 2015), and provided a similar level of validation of the approach by identifying the expected alterations to regional functional connectivity that occur with sleep onset. However, a detailed understanding of the origin of the temporal dynamics of functional connectivity remains elusive. Where some studies have suggested the functional importance of dynamic connectivity because a static correlation appears to be driven by transient periods of strong connection (Allan et al., 2015; Liu and Duyn, 2013) others have recently suggested that dynamic measures are low on neurophysiological meaning and dominated by sampling variability and head motion (Laumann et al., 2016). By directly relating variability in neuronal activity to short-term fluctuations in BOLD signal, we believe our findings of dynamic alpha-BOLD coupling, alongside other sliding-window EEG-fMRI studies (Chang et al., 2013; Tagliazucchi et al., 2012; Yu et al., 2016),

provide some validation for dynamic correlations of BOLD signal reflecting functionally relevant neurophysiological information.

Although in the current study we cannot discount the possibility that spurious correlations can arise when measuring correlations on short time scales, by correcting BOLD data for physiological noise, discarding epochs with high correlations between head-motion and alpha power and also accounting for eye movement/blink events, we have taken considerable measures to minimize the potential for our dynamic correlations being confounded by noise. Although a considerable improvement over static correlations or windows of several minutes, our 16s epoch analysis remains some distance away from the true time scale of brain dynamics. The recent advent of accelerated fMRI acquisition techniques (Feinberg et al., 2010) provides substantial increases in temporal resolution (TR <1s) and the ability to filter out unaliased physiological noise. These advances will make dynamic multimodal neuroimaging strategies like the one described here more powerful and more common (Lee et al., 2013), although the slow temporal properties of the haemodynamic response will always restrict the ability of BOLD fMRI for capturing instantaneous neural events. With such increases in imaging speed comes the necessity to maintain accurate modelling of the HRF, especially for EEG-fMRI where the transfer function mapping neuronal to haemodynamic signals remains an area of active investigation (Rosa et al., 2010). Here we assume the same HRF for all brain regions, although acknowledging this may be suboptimal in the thalamus where different response shapes have been reported (de Munck et al., 2007; Wu et al., 2010).

Eye blinks and eye movements represent an important source of variance in both cognitive state and electrophysiological signals. However, whilst sustained eye closure enhances alpha synchronization and power (Berger, 1929; Feige et al., 2005; Jasper, 1936; Mo et al., 2012) the effect of eye blinks and movements on EEG signals is less clear (Bonfiglio et al., 2011; Gasser et al., 1985; Hagemann and Naumann, 2001). Interestingly, our analysis incorporating eye movements further highlighted the dissociation between the BOLD signals of the PV and LV: the PV was positively correlated with both EB and EM, whilst the LV was negatively correlated with EB and weakly positively correlated with EM. Furthermore the positive responses to both EB and EM that occurred in both the PV and thalamus further demonstrates instances when the BOLD signal is coherent between these two regions, and not always anticorrelated as static alpha-BOLD correlations would suggest (Fig 1). In combination with the lack of a correlation between epoch measures of alpha and EB/EM, the minimal effect of including EB/EM regressors on the alpha-BOLD correlation statistics, and our ICA separation of ocular and alpha activities, these results suggest it is unlikely that ocular modulations of alpha power could be solely responsible for fluctuations in alpha power, and the spatiotemporal variability in alpha-BOLD correlations which we observe. Although a potential limitation of this analysis is that we only consider the power of eye components and not variations in the blink duration which could potentially modulate alpha.

Our GLM analyses revealed the brain areas whose activity correlated with the magnitude of EEG derived EB and EM measures, not just the occurrence of them. The substantial size and extent of BOLD activations to EB and EM suggests that a heterogeneous distribution of EB and EM between experimental conditions could present a troublesome

source of noise in studies of visual processing. We suggest that EB and EM power could be incorporated as additional nuisance regressors in GLM analyses of EEG-fMRI data to account for BOLD signal fluctuations unrelated to the neuronal activity of task processing, or to investigate the interaction between eye movements and brain responses and behavior.

Finally, short-window based analyses offer advantages for assessing the relationship between simultaneously recorded EEG-BOLD signals. Evaluating correlations across continuous time periods of several minutes risks introducing spurious correlations as confounds can arise from using continuous timeseries regressors of EEG power which are sensitive to both transient artefactual and stimulus-locked head-motion (Chowdhury et al., 2014; Jansen et al., 2012) and also to the residual MR artefacts which are routinely left behind by post-processing methods used for artefact correction. Studying dynamic correlations reduces the influence of any single, noisy period on the results and also enables rejection of artefactual epochs from the dataset.

Conclusion

Studying static alpha-BOLD correlations assumes that activity of all regions remains coherent throughout the scan duration, across functionally distinct ICNs, which contradicts current understanding of these ICN's intrinsically dynamic activity. Our findings are consistent with recent work describing temporally distinct patterns of activity occurring at rest (Smith et al., 2012; Zalesky et al., 2014), such that two ICNs, as well as different regions of the same ICN, vary between states of coherent and uncorrelated

activity. In addition, differential recruitment of ICN coherence between trials of a perceptual or cognitive task has a substantial impact on the success or failure of performance (Cocchi et al., 2013; Cohen and van Gaal, 2013). Therefore this work highlights the potential for using dynamic EEG-BOLD relationships to inform trial-by-trial study of the relationship between spontaneous, ongoing electrophysiological processes and behavioural or brain response outcomes (Bassett et al., 2011; Damaraju et al., 2014; Mayhew et al., 2013a; Mayhew et al., 2013b; Schaefer et al., 2014) and investigation of transitions between cognitive states such as switching of attention or the frequent alterations in consciousness that occur during different sleep stages(Hobson and Pace-Schott, 2002; Wilson et al., 2015).

In summary this work demonstrates that alpha-BOLD correlations can be accurately studied at time-scales as short as 16s and that fluctuations in alpha power were not consistently correlated with the BOLD signal, such that the spatial pattern of correlated brain regions fluctuated over time, as a function of alpha power amplitude and relative to the amplitude of stimulus responses. Further work, featuring shorter TR BOLD acquisitions should investigate exactly what time window provides the best representation of EEG-BOLD coupling for specific frequency bands, combining optimal temporal resolution with signal-to-noise considerations. Taken together these findings suggest that the dynamic alpha-BOLD relationship carries a considerable amount of information which could be used to further understand the role of the alpha oscillation in brain function during rest and task performance.

Acknowledgments

This work was supported by the Engineering and Physical Science Research Council (EPSRC) for funding this research (APB EP/F023057/1, EP/J002909/1. SDM was funded by an EPSRC Fellowship (EP/I022325/1) and a Birmingham Fellowship.

Figure Captions

Figure 1. Group average statistical map (A) of the brain regions exhibiting significant static positive (red-yellow) and negative (blue) correlation between the entire 6-minute timecourses of BOLD signal and alpha power. In the lower rows are superimposed the brain regions where alpha-BOLD correlation strength covaries with between-subject variability in IAP (1B, purple) and IAF (1C,green). All images were cluster corrected at $p<0.05$.

Figure 2. A) Group mean alpha-BOLD correlation in each ICN ROI for static (black) and 60s, 32s, 16s and 8s dynamic (white, yellow, green, grey) epoch calculations demonstrating the high similarity in regional alpha-BOLD correlation between different window lengths. Error bars represent standard error in the mean. B) Group mean statistical map of 16s dynamic positive (red-yellow) and negative (blue) alpha-BOLD correlation calculated using random effects, $p<0.001$ uncorrected.

Figure 3. Group mean proportion of 16s epochs that exhibit magnitude of dynamic correlation $R > 0$ (A) or $R > 0.5$ (B). Error bars represent standard error in the mean. Group histograms of dynamic correlations for each ROI are shown in Figure S6. In all cases the correlation values cover the full available range (i.e., -1 to +1), and in the majority of regions, the distribution of R-values approximated a normal distribution. A bias towards a larger proportion of negative R-value epochs was seen for PV, LV and

SM, and to a lesser extent for the IPS, whereas a slight bias towards a majority of positive values was observed for THL and also the PCC and mPFC DMN regions. However it is evident from the distributions that a considerable proportion of epochs displayed dynamic alpha-BOLD correlations of the opposite polarity to that seen in the static correlations

Figure 4. Pie chart examining the group mean proportion of epochs with specific regional combinations of alpha-BOLD relationships. The purple segment at the top represents the proportion of epochs during which the PV,LV,IPS, PCC and THL exhibited dynamic correlations with the same polarity as observed in the static correlation map. Moving clockwise from the top represents gradually decreasing similarity with the spatial pattern of static correlations. The first six segments (cold colours, purple to grey) represent the proportion of the time when PV was negatively correlated with alpha power, coinciding with various other regional correlations, as marked by the solid arc. The remaining three segments (warm colours, yellow to red) explore combinations of positive alpha-PV correlations with other regional correlations, as marked by the dotted arc. The dashed arrow represents the proportion of the time that alpha was simultaneously correlated negatively with PV, LV and IPS.

Figure 5. Mapping unusual alpha-BOLD coupling configurations. Four examples are shown of the group mean maps of voxel-wise alpha-BOLD correlations calculated during epochs where the following correlations were observed: (A) positive alpha-BOLD correlations with LV, (B) positive with PV, (C) negative with THAL and (D) negative with PCC. These maps display some of the variety of configurations, all diverging from

the static average, that alpha-BOLD coupling passes through during a 6-minute resting-state scan.

Figure 6. Dynamic alpha-BOLD correlations are dependent upon alpha power. A) Group mean 16s dynamic correlation for each ROI for lower (white) and upper (grey) thirds of alpha power epochs. Error bars represent standard error in the mean. * denotes significant difference ($p<0.05$) between upper and lower alpha power. Group average maps of negative (B) and positive (C) alpha-BOLD correlation during lower (blue) and upper (red/yellow) alpha power epochs calculated using random effects, $p<0.001$ uncorrected. Green shows the conjunction of the two maps.

Figure 7. Group average maps of positive (A) and negative (B) correlation between BOLD signal and eye blink power and positive BOLD correlation with eye movement power (C). All images were cluster corrected at $p<0.05$.

Figure 8. Group mean dynamic alpha-BOLD negative correlations in rV1 (A), PV+LV (B), IPS (C) and INS (D) ROIs measured at 9 timepoints pre-, peri and post-visual stimulation, sorted into lower (blue) and upper (red) 25% quartiles of BOLD response amplitude. Spatial maps of the dynamic alpha-BOLD negative correlations observed for these quartiles are shown above at five example time-points. Lower quartile (blue) is plotted on top of upper quartile (red) with regions of significant difference additionally superimposed in green. Group mean rV1 BOLD responses from the corresponding

quartiles are plotted in E) illustrating the large difference in response associated with the different temporal profiles of alpha-BOLD negative correlation.

Figure S1. Spatial topographies of the static alpha ICs retained to form the basis of posterior alpha power measurement in twelve representative subjects.

Figure S2. Spatial topography and stacked activity plots for eye-blink (A) and eye-movement (B) independent components extracted from the resting-state EEG of four representative subjects. For display purposes only, the periods in the stacked plots were arbitrarily defined from consecutive 2s sections of spontaneous EEG activity.

Figure S3. Spatial maps of sensorimotor (A), auditory (B), primary visual (C), lateral visual (D), default mode (E), dorsal attention (F) and saliency (G) ICNs identified from group ICA of the resting-state BOLD data. Individual ICN nodes were used as ROIs to extract resting-state BOLD signal and compute regional alpha-BOLD correlations.

Figure S4. Group level maps of significant correlation between BOLD signal and RVT (A) and HRI (B). All images were cluster corrected at $p<0.05$.

Figure S5. For each ROI, a significant correlation is observed between the strength of static alpha-BOLD correlation and the number of epochs exhibiting either a negative (A) or positive (B) dynamic alpha-BOLD correlation.

Figure S6. Histograms showing the distribution of dynamic alpha-BOLD correlations collated over the group for all 16s epochs, for each ROI.

Figure S7. For each subject, the proportion of 16s epochs with alpha power above (white) or below (grey) the mean value of the whole timecourse.

References

Allan, T.W., Francis, S.T., Caballero-Gaudes, C., Morris, P.G., Liddle, E.B., Liddle, P.F., Brookes, M.J., Gowland, P.A., 2015. Functional Connectivity in MRI Is Driven by Spontaneous BOLD Events. PLoS One 10, e0124577.

Allen, E.A., Damaraju, E., Plis, S.M., Erhardt, E.B., Eichele, T., Calhoun, V.D., 2014. Tracking whole-brain connectivity dynamics in the resting state. Cereb Cortex 24, 663-676.

Babiloni, C., Vecchio, F., Bultrini, A., Luca Romani, G., Rossini, P.M., 2006. Pre- and poststimulus alpha rhythms are related to conscious visual perception: a high-resolution EEG study. Cereb Cortex 16, 1690-1700.

Basar, E., Basar-Eroglu, C., Karakas, S., Schurmann, M., 2001. Gamma, alpha, delta, and theta oscillations govern cognitive processes. Int J Psychophysiol 39, 241-248.

Basar, E., Schurmann, M., Basar-Eroglu, C., Karakas, S., 1997. Alpha oscillations in brain functioning: an integrative theory. Int J Psychophysiol 26, 5-29.

Bassett, D.S., Wymbs, N.F., Porter, M.A., Mucha, P.J., Carlson, J.M., Grafton, S.T., 2011. Dynamic reconfiguration of human brain networks during learning. Proc Natl Acad Sci U S A 108, 7641-7646.

Bastos, A.M., Vezoli, J., Bosman, C.A., Schoffelen, J.M., Oostenveld, R., Dowdall, J.R., De Weerd, P., Kennedy, H., Fries, P., 2015. Visual areas exert feedforward and feedback influences through distinct frequency channels. Neuron 85, 390-401.

Becker, R., Reinacher, M., Freyer, F., Villringer, A., Ritter, P., 2011. How Ongoing Neuronal Oscillations Account for Evoked fMRI Variability. Journal of Neuroscience 31, 11016-11027.

Beckmann, C.F., Smith, S.M., 2004. Probabilistic independent component analysis for functional magnetic resonance imaging. IEEE Trans Med Imaging 23, 137-152.

Ben-Simon, E., Podlipsky, I., Arieli, A., Zhdanov, A., Hendler, T., 2008. Never resting brain: simultaneous representation of two alpha related processes in humans. PLoS One 3, e3984.

Berger, H., 1929. Uber das elektroenkephalogram des menschen. Arch Psychiatr Nevenkr 87, 527-570.

Betti, V., Della Penna, S., de Pasquale, F., Mantini, D., Marzetti, L., Romani, G.L., Corbetta, M., 2013. Natural scenes viewing alters the dynamics of functional connectivity in the human brain. Neuron 79, 782-797.

Betzel, R.F., Fukushima, M., He, Y., Zuo, X.N., Sporns, O., 2016. Dynamic fluctuations coincide with periods of high and low modularity in resting-state functional brain networks. Neuroimage 127, 287-297.

Birn, R.M., Murphy, K., Bandettini, P.A., 2008. The effect of respiration variations on independent component analysis results of resting state functional connectivity. Hum Brain Mapp 29, 740-750.

Bodenmann, S., Rusterholz, T., Durr, R., Stoll, C., Bachmann, V., Geissler, E., Jaggi-Schwarz, K., Landolt, H.P., 2009. The functional Val158Met polymorphism of COMT predicts interindividual differences in brain alpha oscillations in young men. J Neurosci 29, 10855-10862.

Bollimunta, A., Chen, Y., Schroeder, C.E., Ding, M., 2008. Neuronal mechanisms of cortical alpha oscillations in awake-behaving macaques. J Neurosci 28, 9976-9988.
Bollimunta, A., Mo, J., Schroeder, C.E., Ding, M., 2011. Neuronal mechanisms and attentional modulation of corticothalamic alpha oscillations. J Neurosci 31, 4935-4943.
Boly, M., Balteau, E., Schnakers, C., Degueldre, C., Moonen, G., Luxen, A., Phillips, C., Peigneux, P., Maquet, P., Laureys, S., 2007. Baseline brain activity fluctuations predict somatosensory perception in humans. Proc Natl Acad Sci U S A 104, 12187-12192.
Bonfiglio, L., Sello, S., Carboncini, M.C., Arrighi, P., Andre, P., Rossi, B., 2011. Reciprocal dynamics of EEG alpha and delta oscillations during spontaneous blinking at rest: a survey on a default mode-based visuo-spatial awareness. Int J Psychophysiol 80, 44-53.
Bristow, D., Frith, C., Rees, G., 2005. Two distinct neural effects of blinking on human visual processing. Neuroimage 27, 136-145.
Brookes, M.J., Woolrich, M., Luckhoo, H., Price, D., Hale, J.R., Stephenson, M.C., Barnes, G.R., Smith, S.M., Morris, P.G., 2011. Investigating the electrophysiological basis of resting state networks using magnetoencephalography. Proceedings of the National Academy of Sciences 108, 16783-16788.
Buffalo, E.A., Fries, P., Landman, R., Buschman, T.J., Desimone, R., 2011. Laminar differences in gamma and alpha coherence in the ventral stream. Proc Natl Acad Sci U S A 108, 11262-11267.
Capotosto, P., Babiloni, C., Romani, G.L., Corbetta, M., 2009. Frontoparietal cortex controls spatial attention through modulation of anticipatory alpha rhythms. J Neurosci 29, 5863-5872.
Chang, C., Cunningham, J.P., Glover, G.H., 2009. Influence of heart rate on the BOLD signal: the cardiac response function. Neuroimage 44, 857-869.
Chang, C., Glover, G.H., 2009. Effects of model-based physiological noise correction on default mode network anti-correlations and correlations. Neuroimage 47, 1448-1459.
Chang, C., Glover, G.H., 2010. Time-frequency dynamics of resting-state brain connectivity measured with fMRI. Neuroimage 50, 81-98.
Chang, C., Liu, Z., Chen, M.C., Liu, X., Duyn, J.H., 2013. EEG correlates of time-varying BOLD functional connectivity. Neuroimage 72, 227-236.
Chowdhury, M.E., Mullinger, K.J., Glover, P., Bowtell, R., 2014. Reference layer artefact subtraction (RLAS): a novel method of minimizing EEG artefacts during simultaneous fMRI. Neuroimage 84, 307-319.
Cocchi, L., Zalesky, A., Fornito, A., Mattingley, J.B., 2013. Dynamic cooperation and competition between brain systems during cognitive control. Trends Cogn Sci 17, 493-501.
Cohen, M.X., van Gaal, S., 2013. Dynamic interactions between large-scale brain networks predict behavioral adaptation after perceptual errors. Cereb Cortex 23, 1061-1072.
Cole, 2010. Advances and pitfalls in the analysis and interpretation of resting-state FMRI data. Frontiers in Systems Neuroscience.
Damaraju, E., Allen, E.A., Belger, A., Ford, J.M., McEwen, S., Mathalon, D.H., Mueller, B.A., Pearlson, G.D., Potkin, S.G., Preda, A., Turner, J.A., Vaidya, J.G., van Erp, T.G., Calhoun, V.D., 2014. Dynamic functional connectivity analysis reveals transient states of dysconnectivity in schizophrenia. Neuroimage Clin 5, 298-308.

de Munck, J.C., Gonçalves, S.I., Faes, T.J.C., Kuijer, J.P.A., Pouwels, P.J.W., Heethaar, R.M., Lopes da Silva, F.H., 2008. A study of the brain's resting state based on alpha band power, heart rate and fMRI. Neuroimage 42, 112-121.
de Munck, J.C., Gonçalves, S.I., Huijboom, L., Kuijer, J.P.A., Pouwels, P.J.W., Heethaar, R.M., Lopes da Silva, F.H., 2007. The hemodynamic response of the alpha rhythm: an EEG/fMRI study. Neuroimage 35, 1142-1151.
de Munck, J.C., Gonçalves, S.I., Mammoliti, R., Heethaar, R.M., Lopes da Silva, F.H., 2009. Interactions between different EEG frequency bands and their effect on alpha-fMRI correlations. Neuroimage 47, 69-76.
de Pasquale, F., Della Penna, S., Snyder, A.Z., Lewis, C., Mantini, D., Marzetti, L., Belardinelli, P., Ciancetta, L., Pizzella, V., Romani, G.L., Corbetta, M., 2010. Temporal dynamics of spontaneous MEG activity in brain networks. Proc Natl Acad Sci U S A 107, 6040-6045.
Eichele, T., Debener, S., Calhoun, V.D., Specht, K., Engel, A.K., Hugdahl, K., von Cramon, D.Y., Ullsperger, M., 2008. Prediction of human errors by maladaptive changes in event-related brain networks. Proc Natl Acad Sci U S A 105, 6173-6178.
Feige, B., Scheffler, K., Esposito, F., Di Salle, F., Hennig, J., Seifritz, E., 2005. Cortical and subcortical correlates of electroencephalographic alpha rhythm modulation. J Neurophysiol 93, 2864-2872.
Feinberg, D.A., Moeller, S., Smith, S.M., Auerbach, E., Ramanna, S., Gunther, M., Glasser, M.F., Miller, K.L., Ugurbil, K., Yacoub, E., 2010. Multiplexed echo planar imaging for sub-second whole brain FMRI and fast diffusion imaging. PLoS One 5, e15710.
Freyer, F., Aquino, K., Robinson, P.A., Ritter, P., Breakspear, M., 2009. Bistability and non-Gaussian fluctuations in spontaneous cortical activity. J Neurosci 29, 8512-8524.
Gao, J.F., Yang, Y., Lin, P., Wang, P., Zheng, C.X., 2010. Automatic removal of eye-movement and blink artifacts from EEG signals. Brain Topogr 23, 105-114.
Gasser, T., Sroka, L., Mocks, J., 1985. The transfer of EOG activity into the EEG for eyes open and closed. Electroencephalogr Clin Neurophysiol 61, 181-193.
Glover, G.H., Li, T.Q., Ress, D., 2000. Image-based method for retrospective correction of physiological motion effects in fMRI: RETROICOR. Magn Reson Med 44, 162-167.
Goldman, R.I., Stern, J.M., Engel, J., Jerome, Cohen, M.S., 2002. Simultaneous EEG and fMRI of the alpha rhythm. Neuroreport 13, 2487-2492.
Goncalves, S.I., de Munck, J.C., Pouwels, P.J., Schoonhoven, R., Kuijer, J.P., Maurits, N.M., Hoogduin, J.M., Van Someren, E.J., Heethaar, R.M., Lopes da Silva, F.H., 2006. Correlating the alpha rhythm to BOLD using simultaneous EEG/fMRI: inter-subject variability. Neuroimage 30, 203-213.
Gonzalez-Castillo, J., Handwerker, D.A., Robinson, M.E., Hoy, C.W., Buchanan, L.C., Saad, Z.S., Bandettini, P.A., 2014. The spatial structure of resting state connectivity stability on the scale of minutes. Front Neurosci 8, 138.
Grandy, T.H., Werkle-Bergner, M., Chicherio, C., Schmiedek, F., Lovden, M., Lindenberger, U., 2013. Peak individual alpha frequency qualifies as a stable neurophysiological trait marker in healthy younger and older adults. Psychophysiology 50, 570-582.
Guipponi, O., Odouard, S., Pinede, S., Wardak, C., Ben Hamed, S., 2014. fMRI Cortical Correlates of Spontaneous Eye Blinks in the Nonhuman Primate. Cereb Cortex.

Haegens, S., Nacher, V., Luna, R., Romo, R., Jensen, O., 2011. alpha-Oscillations in the monkey sensorimotor network influence discrimination performance by rhythmical inhibition of neuronal spiking. Proc Natl Acad Sci U S A 108, 19377-19382.
Hagemann, D., Naumann, E., 2001. The effects of ocular artifacts on (lateralized) broadband power in the EEG. Clin Neurophysiol 112, 215-231.
Handel, B.F., Haarmeier, T., Jensen, O., 2011. Alpha oscillations correlate with the successful inhibition of unattended stimuli. J Cogn Neurosci 23, 2494-2502.
Handwerker, D.A., Roopchansingh, V., Gonzalez-Castillo, J., Bandettini, P.A., 2012. Periodic changes in fMRI connectivity. Neuroimage 63, 1712-1719.
Hanslmayr, S., Aslan, A., Staudigl, T., Klimesch, W., Herrmann, C.S., Bauml, K.H., 2007. Prestimulus oscillations predict visual perception performance between and within subjects. Neuroimage 37, 1465-1473.
Hanslmayr, S., Volberg, G., Wimber, M., Dalal, S.S., Greenlee, M.W., 2013. Prestimulus oscillatory phase at 7 Hz gates cortical information flow and visual perception. Curr Biol 23, 2273-2278.
Hindriks, R., Adhikari, M.H., Murayama, Y., Ganzetti, M., Mantini, D., Logothetis, N.K., Deco, G., 2016. Can sliding-window correlations reveal dynamic functional connectivity in resting-state fMRI? Neuroimage 127, 242-256.
Hindriks, R., Woolrich, M., Luckhoo, H., Joensson, M., Mohseni, H., Kringelbach, M.L., Deco, G., 2015. Role of white-matter pathways in coordinating alpha oscillations in resting visual cortex. Neuroimage 106, 328-339.
Hobson, J.A., Pace-Schott, E.F., 2002. The cognitive neuroscience of sleep: neuronal systems, consciousness and learning. Nat Rev Neurosci 3, 679-693.
Hughes, S.W., Crunelli, V., 2005. Thalamic mechanisms of EEG alpha rhythms and their pathological implications. Neuroscientist 11, 357-372.
Hupe, J.M., Bordier, C., Dojat, M., 2012. A BOLD signature of eyeblinks in the visual cortex. Neuroimage 61, 149-161.
Hutchison, R.M., Womelsdorf, T., Allen, E.A., Bandettini, P.A., Calhoun, V.D., Corbetta, M., Della Penna, S., Duyn, J.H., Glover, G.H., Gonzalez-Castillo, J., Handwerker, D.A., Keilholz, S., Kiviniemi, V., Leopold, D.A., de Pasquale, F., Sporns, O., Walter, M., Chang, C., 2013a. Dynamic functional connectivity: promise, issues, and interpretations. Neuroimage 80, 360-378.
Hutchison, R.M., Womelsdorf, T., Gati, J.S., Everling, S., Menon, R.S., 2013b. Resting-state networks show dynamic functional connectivity in awake humans and anesthetized macaques. Hum Brain Mapp 34, 2154-2177.
Hyvarinen, A., 1999. Fast and robust fixed-point algorithms for independent component analysis. IEEE Trans Neural Netw 10, 626-634.
Jansen, M., White, T.P., Mullinger, K.J., Liddle, E.B., Gowland, P.A., Francis, S.T., Bowtell, R., Liddle, P.F., 2012. Motion-related artefacts in EEG predict neuronally plausible patterns of activation in fMRI data. Neuroimage 59, 261-270.
Jasper, H.H., 1936. Cortical Excitatory State and Variability in Human Brain Rhythms. Science 83, 259-260.
Jenkinson, M., Bannister, P., Brady, M., Smith, S., 2002. Improved optimization for the robust and accurate linear registration and motion correction of brain images. Neuroimage 17, 825-841.

Jensen, O., Gelfand, J., Kounios, J., Lisman, J.E., 2002. Oscillations in the alpha band (9-12 Hz) increase with memory load during retention in a short-term memory task. Cereb Cortex 12, 877-882.
Jensen, O., Mazaheri, A., 2010. Shaping functional architecture by oscillatory alpha activity: gating by inhibition. Front Hum Neurosci 4, 186.
Jung, T.P., Makeig, S., Westerfield, M., Townsend, J., Courchesne, E., Sejnowski, T.J., 2000. Removal of eye activity artifacts from visual event-related potentials in normal and clinical subjects. Clin Neurophysiol 111, 1745-1758.
Keilholz, S.D., Magnuson, M.E., Pan, W.J., Willis, M., Thompson, G.J., 2013. Dynamic properties of functional connectivity in the rodent. Brain Connect 3, 31-40.
Khalsa, S., Mayhew, S.D., Chechlacz, M., Bagary, M., Bagshaw, A.P., 2013. The structural and functional connectivity of the posterior cingulate cortex: Comparison between deterministic and probabilistic tractography for the investigation of structure-function relationships. Neuroimage In Press.
Kiviniemi, V., Vire, T., Remes, J., Elseoud, A.A., Starck, T., Tervonen, O., Nikkinen, J., 2011. A sliding time-window ICA reveals spatial variability of the default mode network in time. Brain Connect 1, 339-347.
Klimesch, W., 1999. EEG alpha and theta oscillations reflect cognitive and memory performance: a review and analysis. Brain Res Brain Res Rev 29, 169-195.
Klimesch, W., Sauseng, P., Hanslmayr, S., 2007. EEG alpha oscillations: the inhibition-timing hypothesis. Brain Res Rev 53, 63-88.
Koch, S.P., Koendgen, S., Bourayou, R., Steinbrink, J., Obrig, H., 2008. Individual alpha-frequency correlates with amplitude of visual evoked potential and hemodynamic response. Neuroimage 41, 233-242.
Kondacs, A., Szabo, M., 1999. Long-term intra-individual variability of the background EEG in normals. Clin Neurophysiol 110, 1708-1716.
Laufs, H., Holt, J.L., Elfont, R., Krams, M., Paul, J.S., Krakow, K., Kleinschmidt, A., 2006. Where the BOLD signal goes when alpha EEG leaves. Neuroimage 31, 1408-1418.
Laufs, H., Kleinschmidt, A., Beyerle, A., Eger, E., Salek-Haddadi, A., Preibisch, C., Krakow, K., 2003. EEG-correlated fMRI of human alpha activity. Neuroimage 19, 1463-1476.
Laumann, T.O., Snyder, A.Z., Mitra, A., Gordon, E.M., Gratton, C., Adeyemo, B., Gilmore, A.W., Nelson, S.M., Berg, J.J., Greene, D.J., McCarthy, J.E., Tagliazucchi, E., Laufs, H., Schlaggar, B.L., Dosenbach, N.U., Petersen, S.E., 2016. On the Stability of BOLD fMRI Correlations. Cereb Cortex.
Lee, H.L., Zahneisen, B., Hugger, T., LeVan, P., Hennig, J., 2013. Tracking dynamic resting-state networks at higher frequencies using MR-encephalography. Neuroimage 65, 216-222.
Leonardi, N., Van De Ville, D., 2015. On spurious and real fluctuations of dynamic functional connectivity during rest. Neuroimage 104, 430-436.
Linkenkaer-Hansen, K., Nikulin, V.V., Palva, S., Ilmoniemi, R.J., Palva, J.M., 2004. Prestimulus oscillations enhance psychophysical performance in humans. J Neurosci 24, 10186-10190.
Liu, X., Duyn, J.H., 2013. Time-varying functional network information extracted from brief instances of spontaneous brain activity. Proc Natl Acad Sci U S A 110, 4392-4397.

Liu, Z., de Zwart, J.A., Yao, B., van Gelderen, P., Kuo, L.W., Duyn, J.H., 2012. Finding thalamic BOLD correlates to posterior alpha EEG. Neuroimage 63, 1060-1069.
Logothetis, N.K., 2002. The neural basis of the blood-oxygen-level-dependent functional magnetic resonance imaging signal. Philos Trans R Soc Lond B Biol Sci 357, 1003-1037.
Lopes da Silva, F., 1991. Neural mechanisms underlying brain waves: from neural membranes to networks. Electroencephalogr Clin Neurophysiol 79, 81-93.
Magri, C., Schridde, U., Murayama, Y., Panzeri, S., Logothetis, N.K., 2012. The amplitude and timing of the BOLD signal reflects the relationship between local field potential power at different frequencies. J Neurosci 32, 1395-1407.
Mantini, D., Perrucci, M.G., Del Gratta, C., Romani, G.L., Corbetta, M., 2007. Electrophysiological signatures of resting state networks in the human brain. Proc Natl Acad Sci U S A 104, 13170-13175.
Mayhew, S.D., Hylands-White, N., Porcaro, C., Derbyshire, S.W., Bagshaw, A.P., 2013a. Intrinsic variability in the human response to pain is assembled from multiple, dynamic brain processes. Neuroimage 75, 68-78.
Mayhew, S.D., Ostwald, D., Porcaro, C., Bagshaw, A.P., 2013b. Spontaneous EEG alpha oscillation interacts with positive and negative BOLD responses in the visual-auditory cortices and default-mode network. Neuroimage 76, 362-372.
Mazaheri, A., Jensen, O., 2010. Shaping Functional Architecture by Oscillatory Alpha Activity: Gating by Inhibition. Frontiers in Human Neuroscience 4, 186.
Mo, J., Liu, Y., Huang, H., Ding, M., 2012. Coupling between visual alpha oscillations and default mode activity. Neuroimage 68C, 112-118.
Moosmann, M., Ritter, P., Krastel, I., Brink, A., Thees, S., Blankenburg, F., Taskin, B., Obrig, H., Villringer, A., 2003. Correlates of alpha rhythm in functional magnetic resonance imaging and near infrared spectroscopy. Neuroimage 20, 145-158.
Mullinger, K.J., Morgan, P.S., Bowtell, R.W., 2008. Improved artifact correction for combined electroencephalography/functional MRI by means of synchronization and use of vectorcardiogram recordings. J Magn Reson Imaging 27, 607-616.
Mullinger, K.J., Yan, W.X., Bowtell, R., 2011. Reducing the gradient artefact in simultaneous EEG-fMRI by adjusting the subject's axial position. Neuroimage 54, 1942-1950.
Napflin, M., Wildi, M., Sarnthein, J., 2007. Test-retest reliability of resting EEG spectra validates a statistical signature of persons. Clin Neurophysiol 118, 2519-2524.
Olbrich, S., Mulert, C., Karch, S., Trenner, M., Leicht, G., Pogarell, O., Hegerl, U., 2009. EEG-vigilance and BOLD effect during simultaneous EEG/fMRI measurement. Neuroimage 45, 319-332.
Oostenveld, R., Fries, P., Maris, E., Schoffelen, J.M., 2011. FieldTrip: Open source software for advanced analysis of MEG, EEG, and invasive electrophysiological data. Comput Intell Neurosci 2011, 156869.
Ostwald, D., Porcaro, C., Bagshaw, A.P., 2010. An information theoretic approach to EEG-fMRI integration of visually evoked responses. Neuroimage 49, 498-516.
Palva, S., Palva, J.M., 2011. Functional roles of alpha-band phase synchronization in local and large-scale cortical networks. Front Psychol 2, 204.
Pfurtscheller, G., Lopes da Silva, F.H., 1999. Event-related EEG/MEG synchronization and desynchronization: basic principles. Clin Neurophysiol 110, 1842-1857.

Plochl, M., Ossandon, J.P., Konig, P., 2012. Combining EEG and eye tracking: identification, characterization, and correction of eye movement artifacts in electroencephalographic data. Front Hum Neurosci 6, 278.
Porcaro, C., Ostwald, D., Bagshaw, A.P., 2010. Functional source separation improves the quality of single trial visual evoked potentials recorded during concurrent EEG-fMRI. Neuroimage 50, 112-123.
Przezdzik, I., Bagshaw, A.P., Mayhew, S.D., 2013. Some brains are more strongly functionally connected than others: a resting-state fMRI study of inter and intra network coherence. Proc ISMRM 2262.
Rihs, T.A., Michel, C.M., Thut, G., 2007. Mechanisms of selective inhibition in visual spatial attention are indexed by alpha-band EEG synchronization. Eur J Neurosci 25, 603-610.
Rihs, T.A., Michel, C.M., Thut, G., 2009. A bias for posterior alpha-band power suppression versus enhancement during shifting versus maintenance of spatial attention. Neuroimage 44, 190-199.
Romei, V., Brodbeck, V., Michel, C., Amedi, A., Pascual-Leone, A., Thut, G., 2008. Spontaneous fluctuations in posterior alpha-band EEG activity reflect variability in excitability of human visual areas. Cereb Cortex 18, 2010-2018.
Rosa, M.J., Kilner, J., Blankenburg, F., Josephs, O., Penny, W., 2010. Estimating the transfer function from neuronal activity to BOLD using simultaneous EEG-fMRI. Neuroimage 49, 1496-1509.
Roth, B., 1961. The clinical and theoretical importance of EEG rhythms corresponding to states of lowered vigilance. Electroencephalogr Clin Neurophysiol 13, 395-399.
Roux, F., Wibral, M., Singer, W., Aru, J., Uhlhaas, P.J., 2013. The phase of thalamic alpha activity modulates cortical gamma-band activity: evidence from resting-state MEG recordings. J Neurosci 33, 17827-17835.
Sadaghiani, S., Hesselmann, G., Kleinschmidt, A., 2009. Distributed and Antagonistic Contributions of Ongoing Activity Fluctuations to Auditory Stimulus Detection. Journal of Neuroscience 29, 13410-13417.
Sadaghiani, S., Poline, J.B., Kleinschmidt, A., D'Esposito, M., 2015. Ongoing dynamics in large-scale functional connectivity predict perception. Proc Natl Acad Sci U S A 112, 8463-8468.
Sauseng, P., Klimesch, W., Doppelmayr, M., Pecherstorfer, T., Freunberger, R., Hanslmayr, S., 2005. EEG alpha synchronization and functional coupling during top-down processing in a working memory task. Hum Brain Mapp 26, 148-155.
Schaefer, A., Margulies, D.S., Lohmann, G., Gorgolewski, K.J., Smallwood, J., Kiebel, S.J., Villringer, A., 2014. Dynamic network participation of functional connectivity hubs assessed by resting-state fMRI. Front Hum Neurosci 8, 195.
Scheeringa, R., Fries, P., Petersson, K.-M., Oostenveld, R., Grothe, I., Norris, D.G., Hagoort, P., Bastiaansen, M.C.M., 2011a. Neuronal Dynamics Underlying High- and Low-Frequency EEG Oscillations Contribute Independently to the Human BOLD Signal. Neuron 69, 572-583.
Scheeringa, R., Mazaheri, A., Bojak, I., Norris, D.G., Kleinschmidt, A., 2011b. Modulation of visually evoked cortical FMRI responses by phase of ongoing occipital alpha oscillations. J Neurosci 31, 3813-3820.

Schwarzkopf, D.S., Robertson, D.J., Song, C., Barnes, G.R., Rees, G., 2012. The frequency of visually induced gamma-band oscillations depends on the size of early human visual cortex. J Neurosci 32, 1507-1512.
Shakil, S., Lee, C.H., Keilholz, S.D., 2016. Evaluation of sliding window correlation performance for characterizing dynamic functional connectivity and brain states. Neuroimage 133, 111-128.
Singer, W., 1993. Synchronization of cortical activity and its putative role in information processing and learning. Annu Rev Physiol 55, 349-374.
Smith, S.M., Miller, K.L., Moeller, S., Xu, J., Auerbach, E.J., Woolrich, M.W., Beckmann, C.F., Jenkinson, M., Andersson, J., Glasser, M.F., Van Essen, D.C., Feinberg, D.A., Yacoub, E.S., Ugurbil, K., 2012. Temporally-independent functional modes of spontaneous brain activity. Proc Natl Acad Sci U S A 109, 3131-3136.
Strijkstra, A.M., Beersma, D.G., Drayer, B., Halbesma, N., Daan, S., 2003. Subjective sleepiness correlates negatively with global alpha (8-12 Hz) and positively with central frontal theta (4-8 Hz) frequencies in the human resting awake electroencephalogram. Neurosci Lett 340, 17-20.
Tagliazucchi, E., von Wegner, F., Morzelewski, A., Brodbeck, V., Laufs, H., 2012. Dynamic BOLD functional connectivity in humans and its electrophysiological correlates. Front Hum Neurosci 6, 339.
Thompson, G.J., Magnuson, M.E., Merritt, M.D., Schwarb, H., Pan, W.J., McKinley, A., Tripp, L.D., Schumacher, E.H., Keilholz, S.D., 2013a. Short-time windows of correlation between large-scale functional brain networks predict vigilance intraindividually and interindividually. Hum Brain Mapp 34, 3280-3298.
Thompson, G.J., Merritt, M.D., Pan, W.J., Magnuson, M.E., Grooms, J.K., Jaeger, D., Keilholz, S.D., 2013b. Neural correlates of time-varying functional connectivity in the rat. Neuroimage 83, 826-836.
Thut, G., Nietzel, A., Brandt, S.A., Pascual-Leone, A., 2006. Alpha-band electroencephalographic activity over occipital cortex indexes visuospatial attention bias and predicts visual target detection. J Neurosci 26, 9494-9502.
Van Dijk, K.R.A., Hedden, T., Venkataraman, A., Evans, K.C., Lazar, S.W., Buckner, R.L., 2009. Intrinsic Functional Connectivity As a Tool For Human Connectomics: Theory, Properties, and Optimization. Journal of Neurophysiology 103, 297-321.
van Kerkoerle, T., Self, M.W., Dagnino, B., Gariel-Mathis, M.A., Poort, J., van der Togt, C., Roelfsema, P.R., 2014. Alpha and gamma oscillations characterize feedback and feedforward processing in monkey visual cortex. Proc Natl Acad Sci U S A 111, 14332-14341.
Varela, F., Lachaux, J.P., Rodriguez, E., Martinerie, J., 2001. The brainweb: phase synchronization and large-scale integration. Nat Rev Neurosci 2, 229-239.
Vincent, J.L., Patel, G.H., Fox, M.D., Snyder, A.Z., Baker, J.T., Van Essen, D.C., Zempel, J.M., Snyder, L.H., Corbetta, M., Raichle, M.E., 2007. Intrinsic functional architecture in the anaesthetized monkey brain. Nature 447, 83-86.
von Stein, A., Chiang, C., Konig, P., 2000. Top-down processing mediated by interareal synchronization. Proc Natl Acad Sci U S A 97, 14748-14753.
Wilson, R.S., Mayhew, S.D., Rollings, D.T., Goldstone, A., Przezdzik, I., Arvanitis, T.N., Bagshaw, A.P., 2015. Influence of Epoch Length on Measurement of Dynamic

Functional Connectivity in Wakefulness and Behavioural Validation in Sleep. Neuroimage.
Wu, L., Eichele, T., Calhoun, V.D., 2010. Reactivity of hemodynamic responses and functional connectivity to different states of alpha synchrony: a concurrent EEG-fMRI study. Neuroimage 52, 1252-1260.
Yu, Q., Wu, L., Bridwell, D.A., Erhardt, E.B., Du, Y., He, H., Chen, J., Liu, P., Sui, J., Pearlson, G., Calhoun, V.D., 2016. Building an EEG-fMRI Multi-Modal Brain Graph: A Concurrent EEG-fMRI Study. Front Hum Neurosci 10, 476.
Yuan, H., Zotev, V., Phillips, R., Bodurka, J., 2013. Correlated slow fluctuations in respiration, EEG, and BOLD fMRI. Neuroimage 79, 81-93.
Zalesky, A., Fornito, A., Cocchi, L., Gollo, L.L., Breakspear, M., 2014. Time-resolved resting-state brain networks. Proc Natl Acad Sci U S A 111, 10341-10346.
Zhan, Z., Xu, L., Zuo, T., Xie, D., Zhang, J., Yao, L., Wu, X., 2014. The contribution of different frequency bands of fMRI data to the correlation with EEG alpha rhythm. Brain Res 1543, 235-243.
Zhang, Y., Brady, M., Smith, S., 2001. Segmentation of brain MR images through a hidden Markov random field model and the expectation-maximization algorithm. IEEE Trans Med Imaging 20, 45-57.
Zumer, J.M., Scheeringa, R., Schoffelen, J.M., Norris, D.G., Jensen, O., 2014. Occipital alpha activity during stimulus processing gates the information flow to object-selective cortex. PLoS Biol 12, e1001965.

Table 1. Group mean proportion of 16s epochs which exhibited various combinations of regional alpha-BOLD correlations. Each line represents a separate instance of concurrent negative (left) and positive (centre) dynamic alpha-BOLD correlations in different ROIs.

ROIs with negative alpha-BOLD correlation	ROIs with positive alpha-BOLD correlation	Group mean % of total 16s epochs
PV,LV,IPS	PCC, THL	7.7
PV,LV,IPS	PCC	12.9
PV,LV,IPS	THL	16.6
PCC,THL	PV,LV,IPS	0.6
PV,LV,IPS,PCC,THL	-	2.1
PV,LV,IPS	-	35.4
-	PV,LV,IPS	16.4
PV or LV or IPS		83.6
PV,LV,IPS,INS	-	23.1
PV,LV	-	44.5
-	PV,LV	24.9
PV or LV	-	75.1
PV,IPS	-	42.9
LV,IPS	-	44.6
PV,LV	IPS	9.0
PV,IPS	LV	7.4
LV,IPS	PV	9.1
PV,ACC	-	36.1
PV,INS	-	36.6
INS or ACC	PV	20.0
SM	PV	16.2
IPS	PCC	28.3

Highlights

- Studied temporal dynamics of resting-state correlations between alpha EEG and BOLD fMRI
- 16s dynamic correlations represent the static mean pattern only 10% of the total time
- Alpha-BOLD coupling shows many spatial configurations that diverge from the static network
- Regional alpha-BOLD coupling fluctuates over time and depends on alpha power amplitude
- Visual regions, correlated with alpha on average, display different patterns over time

Figure 1

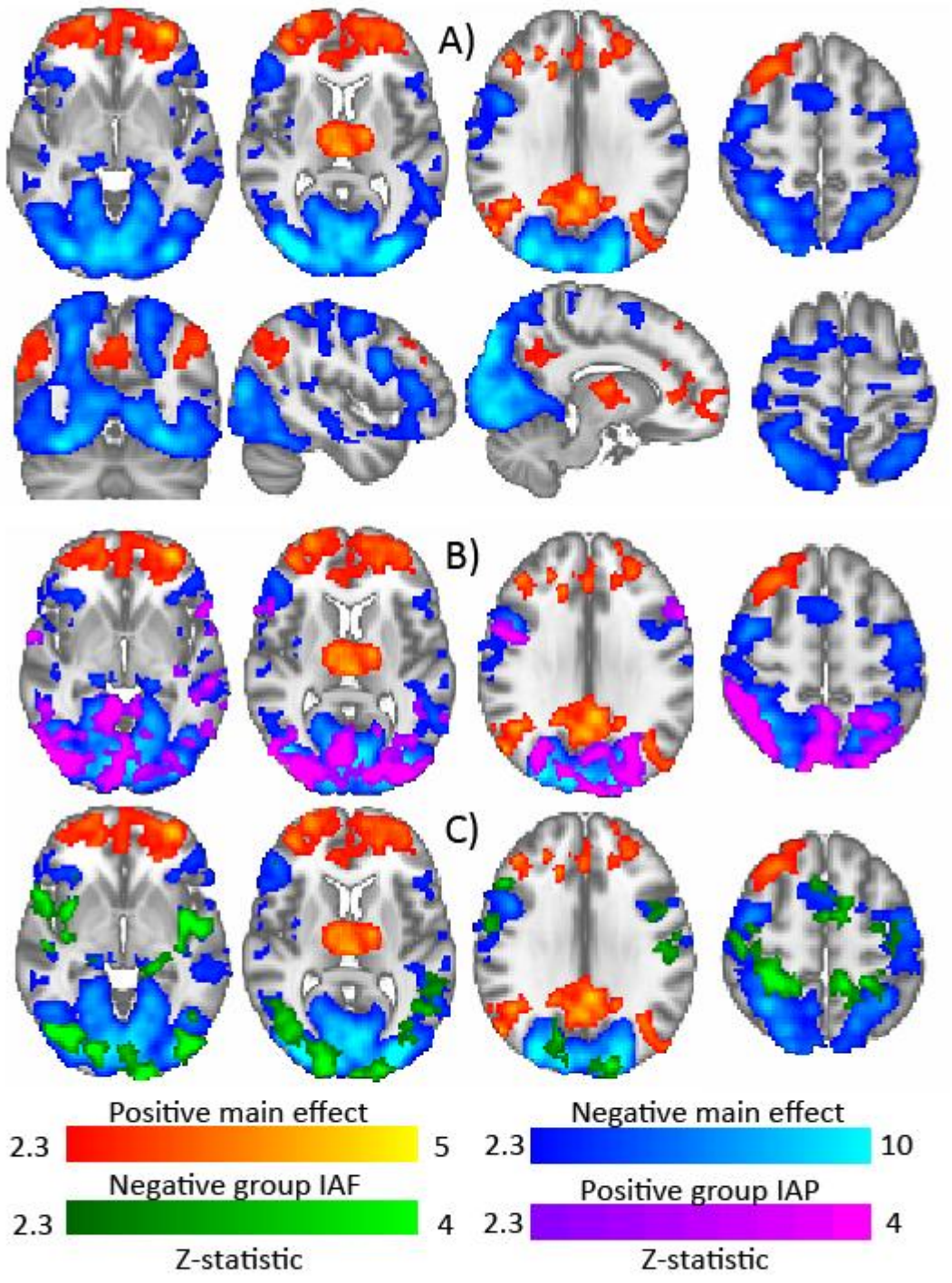
A)
B)
C)
Positive main effect
2.3
5
Negative main effect
2.3
10
Negative group IAF
2.3
4
Positive group IAP
2.3
4
Z-statistic
Z-statistic

Figure 2

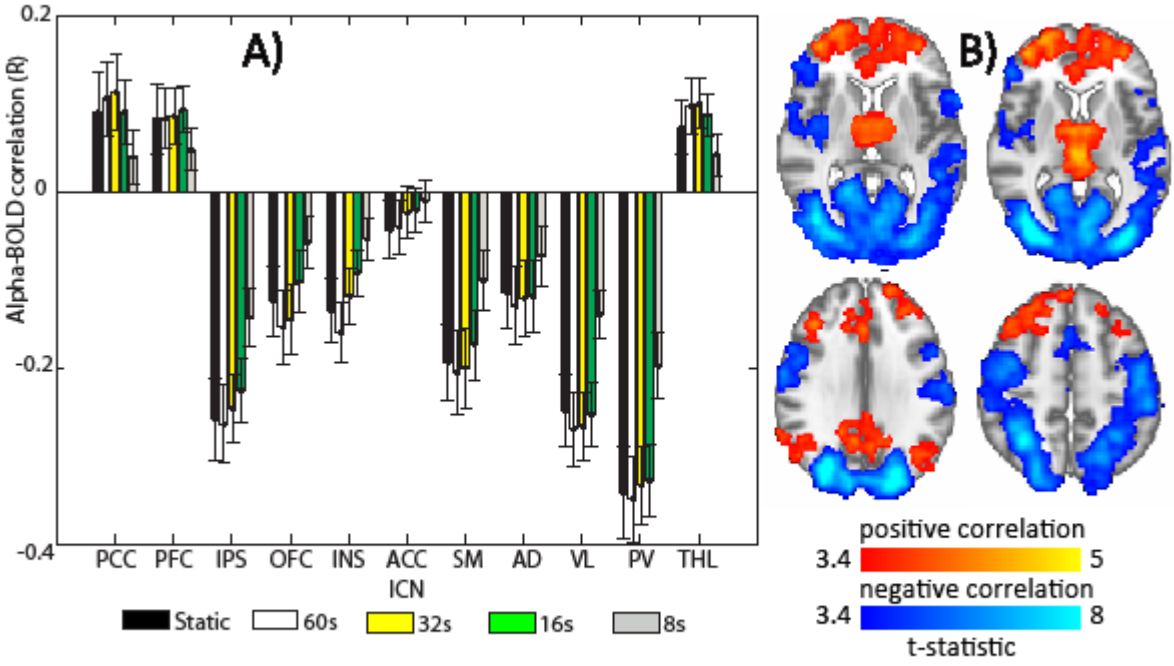
A)
B)
Alpha-BOLD correlation (R)
0.2
0
-0.2
-0.4
PCC
PFC
IPS
OFC
INS
ACC
SM
AD
VL
PV
THL
ICN
Static
60s
32s
16s
8s
positive correlation
3.4
5
negative correlation
3.4
8
t-statistic

Figure 3

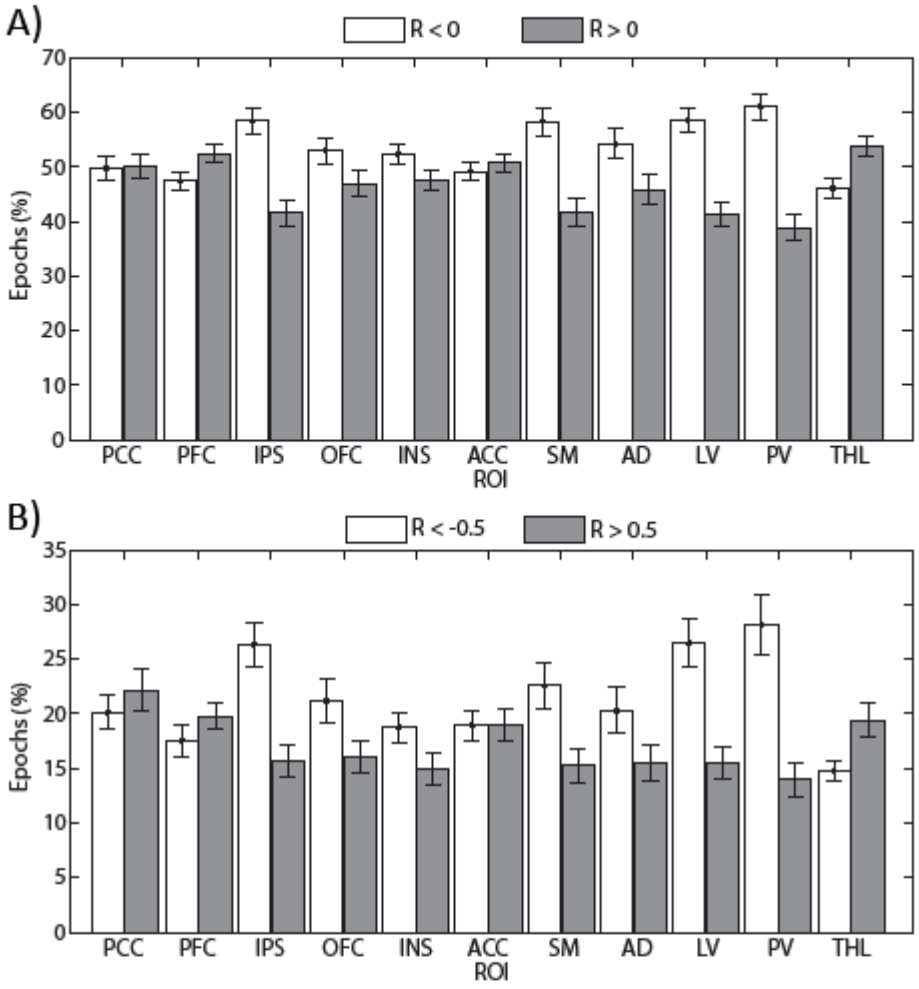
A)
R < 0
R > 0
Epochs (%)
70
60
50
40
30
20
10
0
PCC
PFC
IPS
OFC
INS
ACC
SM
AD
LV
PV
THL
ROI
B)
R < -0.5
R > 0.5
Epochs (%)
35
30
25
20
15
10
5
0
PCC
PFC
IPS
OFC
INS
ACC
SM
AD
LV
PV
THL
ROI

Figure 4

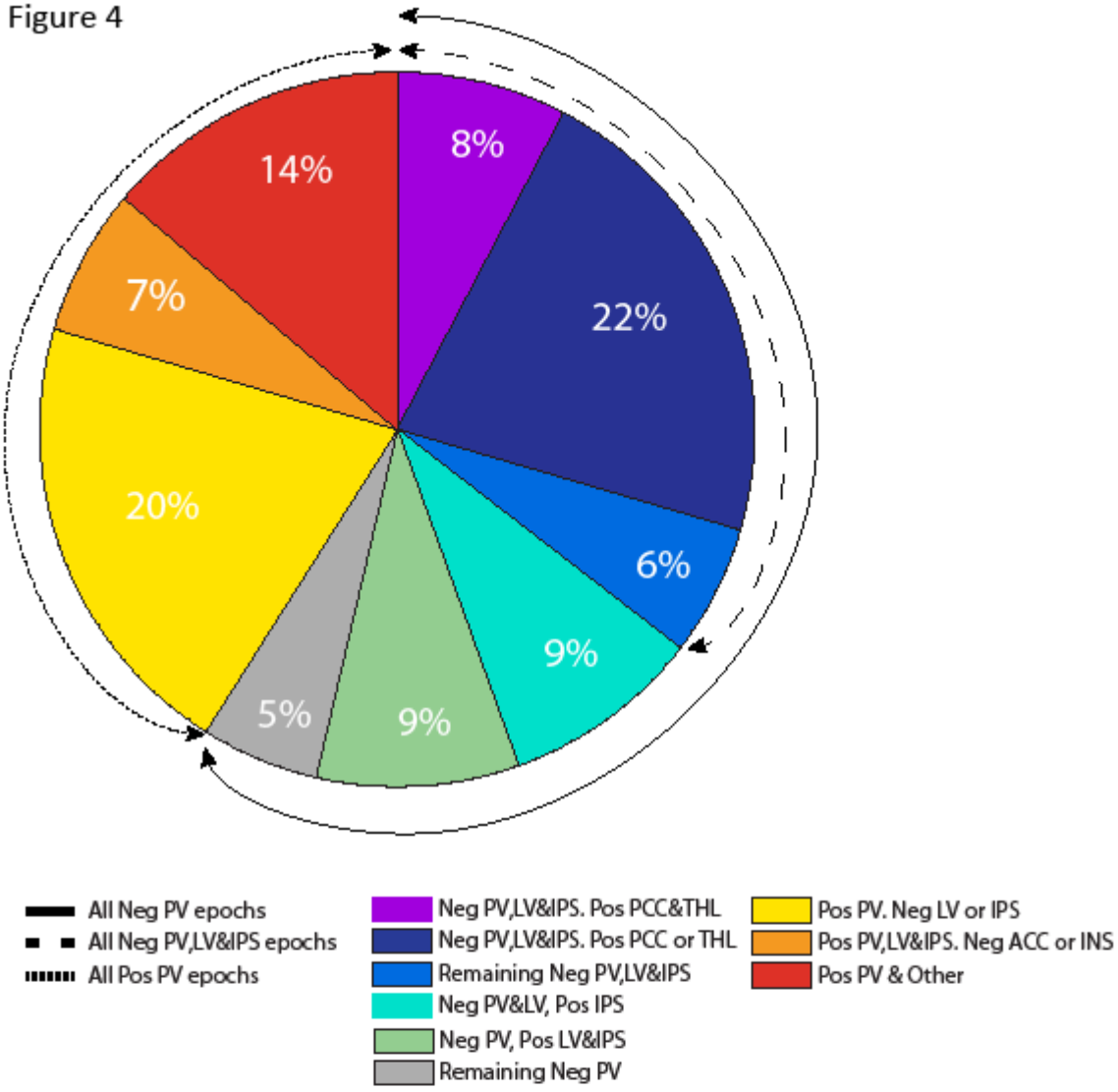
8%
22%
6%
9%
9%
5%
20%
7%
14%
All Neg PV epochs
All Neg PV,LV&IPS epochs
All Pos PV epochs
Neg PV,LV&IPS. Pos PCC&THL
Neg PV,LV&IPS. Pos PCC or THL
Remaining Neg PV,LV&IPS
Neg PV&LV, Pos IPS
Neg PV, Pos LV&IPS
Remaining Neg PV
Pos PV. Neg LV or IPS
Pos PV,LV&IPS. Neg ACC or INS
Pos PV & Other

Figure 5

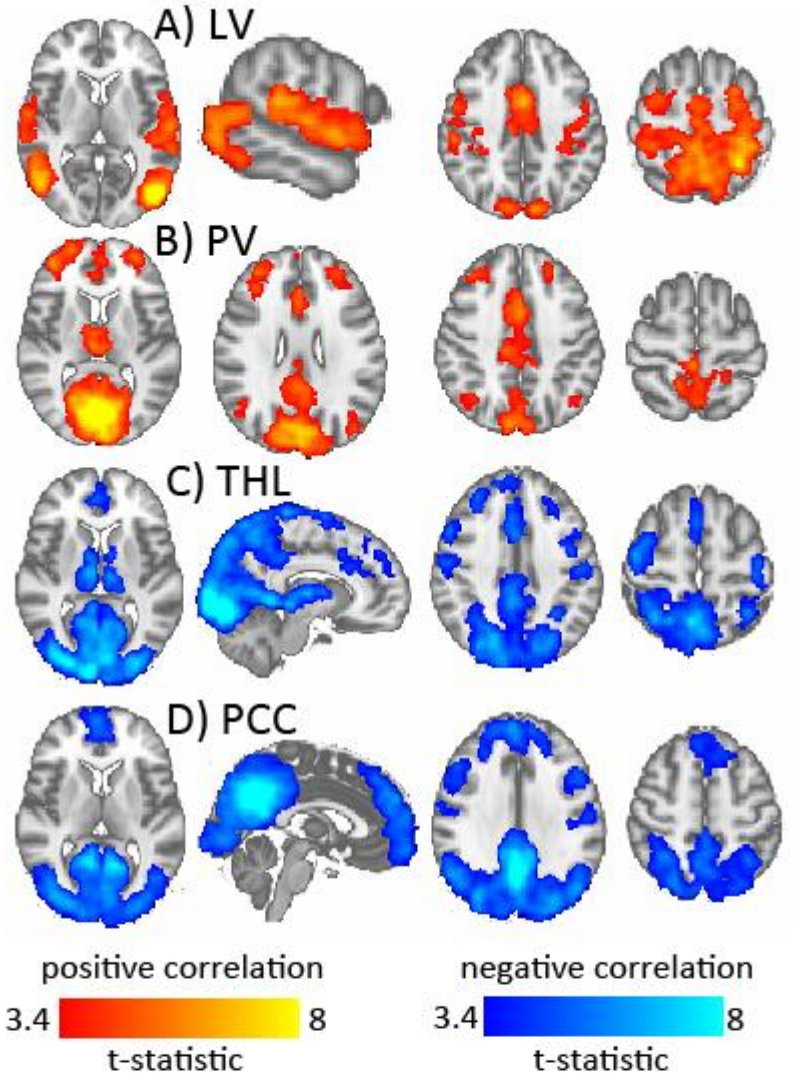
A) LV
B) PV
C) THL
D) PCC
positive correlation
3.4
8
t-statistic
negative correlation
3.4
8
t-statistic

Figure 6

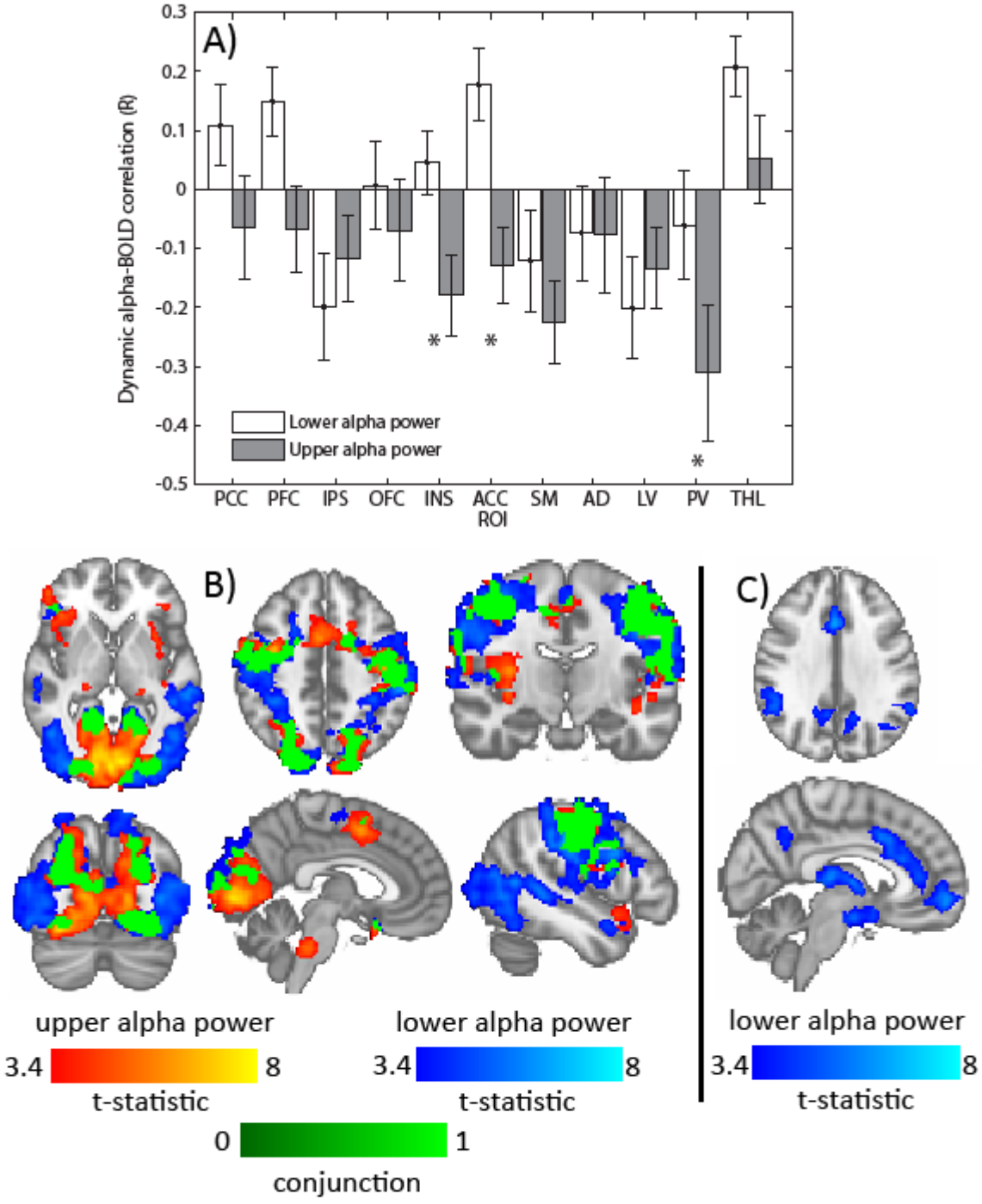
A)
Dynamic alpha-BOLD correlation (R)
0.3
0.2
0.1
0
-0.1
-0.2
-0.3
-0.4
-0.5
Lower alpha power
Upper alpha power
*
*
*
PCC PFC IPS OFC INS ACC SM AD LV PV THL
ROI
B)
C)
upper alpha power
3.4
8
t-statistic
lower alpha power
3.4
8
t-statistic
0
1
conjunction
lower alpha power
3.4
8
t-statistic

Figure 7

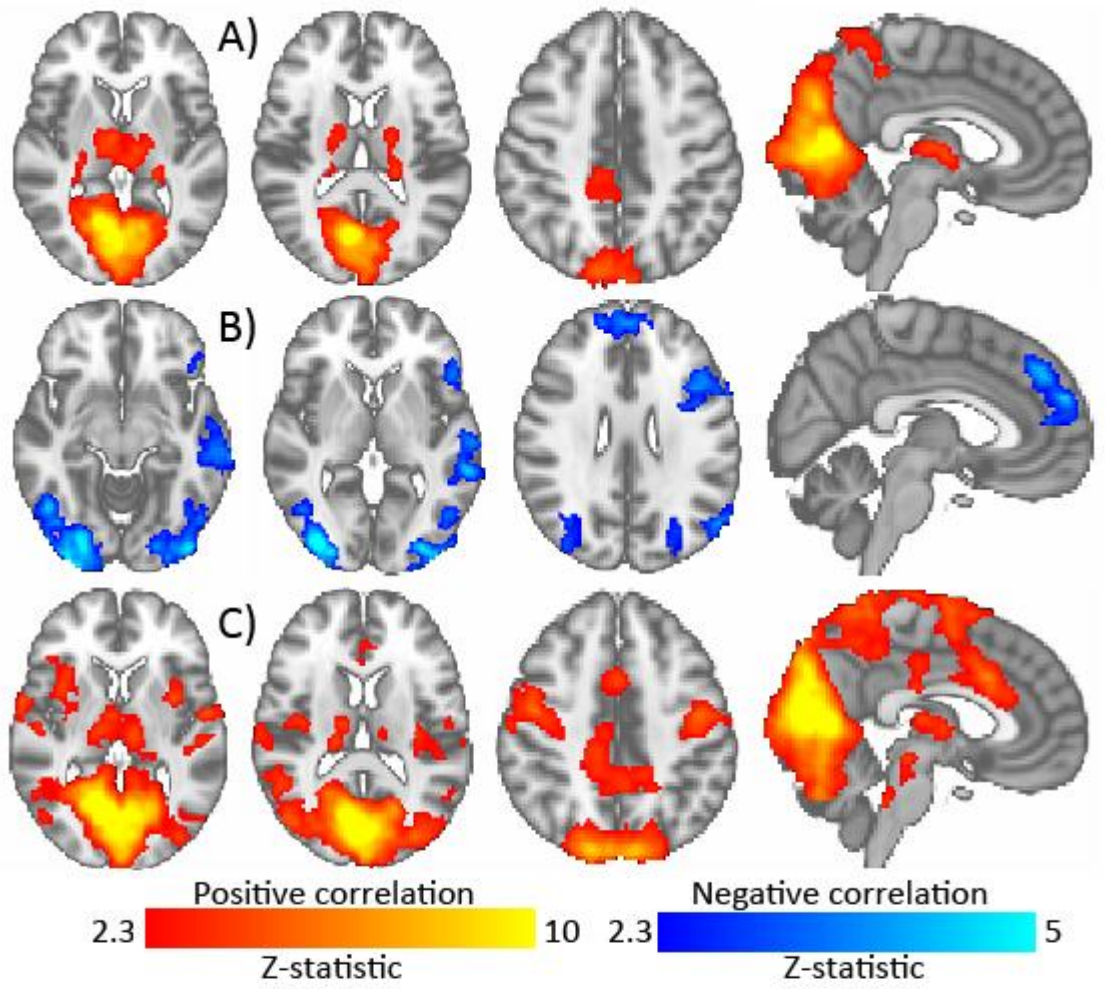
A)
B)
C)
Positive correlation
2.3
10
Z-statistic
Negative correlation
2.3
5
Z-statistic

Figure 8

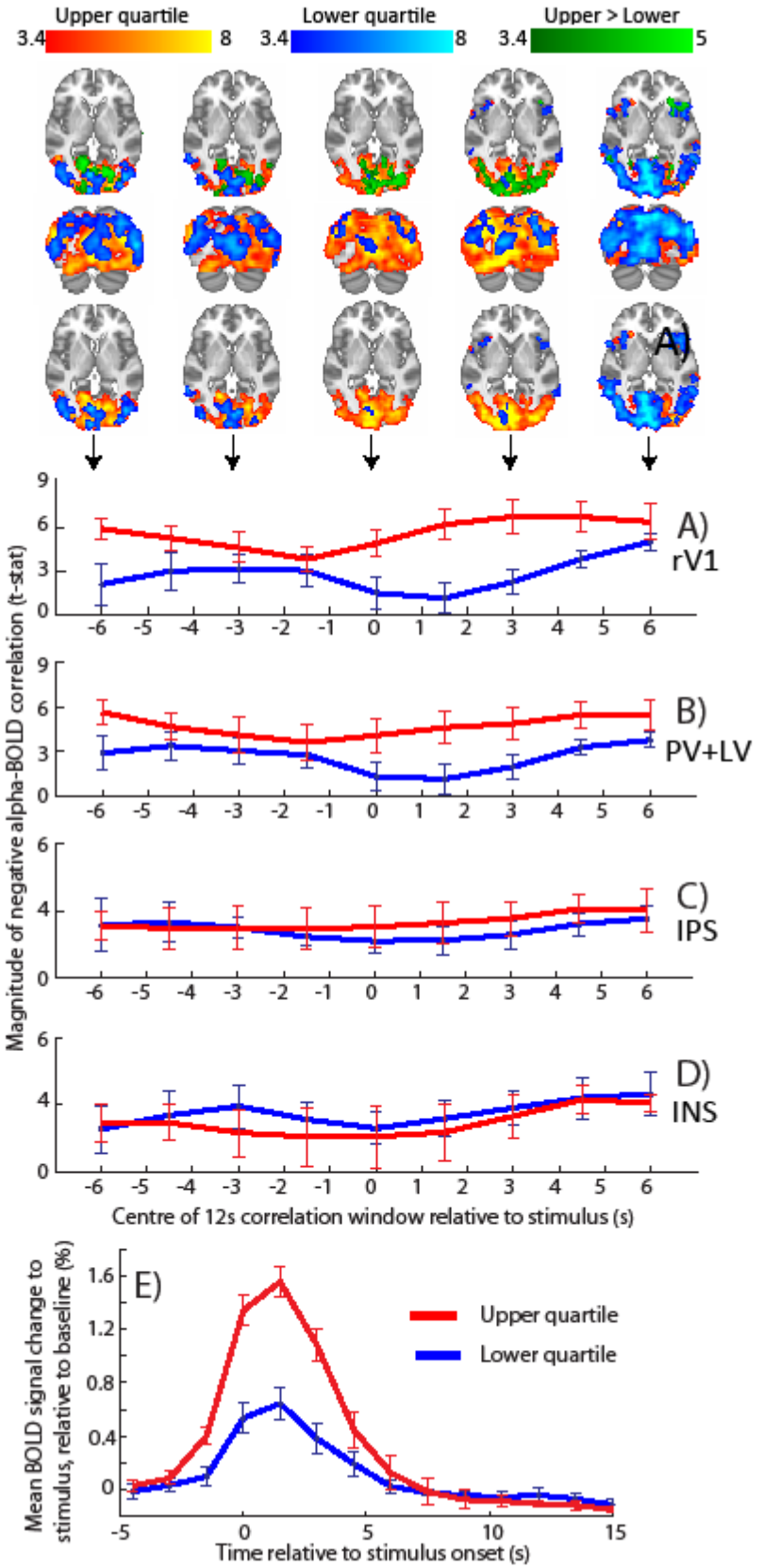
Upper quartile
3.4
8
Lower quartile
3.4
8
Upper > Lower
3.4
5
A)
A)
rV1
B)
PV+LV
C)
IPS
D)
INS
Magnitude of negative alpha-BOLD correlation (t-stat)
Centre of 12s correlation window relative to stimulus (s)
E)
Upper quartile
Lower quartile
Mean BOLD signal change to stimulus, relative to baseline (%)
Time relative to stimulus onset (s)